AGU PUBLICATIONS

JGR

Journal of Geophysical Research: Oceans

RESEARCH ARTICLE

10.1002/2015JC011312

Special Section:
Forum for Arctic Modeling and Observational Synthesis (FAMOS): Results and Synthesis of Coordinated Experiments

Fram Strait and Greenland Sea transports, water masses, and water mass transformations 1999–2010 (and beyond)

Marika Marnela[1,2], Bert Rudels[1], Ilona Goszczko[3], Agnieszka Beszczynska-Möller[3], and Ursula Schauer[4]

[1]Finnish Meteorological Institute, Marine Research, Helsinki, Finland, [2]University of Helsinki, Department of Physics, Helsinki, Finland, [3]Institute of Oceanology, Polish Academy of Sciences, Physical Oceanography Department, Sopot, Poland, [4]Alfred Wegener Institute, Climate Sciences, Bremerhaven, Germany

Abstract The exchanges between the Nordic Seas and the Arctic Ocean are important for the ocean circulation and climate. Transports are here estimated using summer hydrographic data from the Greenland Sea and the Fram Strait. Geostrophic transports are computed from hydrographic sections at 75°N in the Greenland Sea and at about 79°N in the Fram Strait. Geostrophic velocities are adjusted with summer velocities derived from Argo floats, and four conservation constraints are applied to a box closed by the two sections. The estimated net volume transports are 0.8 ± 1.5 Sv southward. Net freshwater transports through the Greenland Sea section are estimated at 54 ± 20 mSv and through the Fram Strait section at 66 ± 9 mSv. Heat loss in the area between the two sections is estimated at 9 ± 12 TW. Convection depths in the Greenland Sea are estimated from observations and vary between about 200 and 2000 dbar showing no trend. Water mass properties in the Greenland Sea are affected both by convection and lateral mixing. Vertical mixing is estimated from hydrography and based on it about 1 Sv of diluted Arctic Ocean waters are estimated to enter the Greenland Sea. The properties of Atlantic, intermediate, and deep waters are studied. Deep water properties are defined using water mass triangles and are subject to decadal changes.

Key Points:
- Constraints are applied on geostrophic velocities adjusted with Argo data to estimate transports
- Mixing is estimated between the Greenland Sea salinity maximum and the deep layer
- Deep water masses are defined using water mass triangles

Correspondence to:
M. Marnela,
marika.marnela@fmi.fi

Citation:
Marnela, M., B. Rudels, I. Goszczko, A. Beszczynska-Möller, and U. Schauer (2016), Fram Strait and Greenland Sea transports, water masses, and water mass transformations 1999–2010 (and beyond), *J. Geophys. Res. Oceans*, *121*, 2314–2346, doi:10.1002/2015JC011312.

Received 10 SEP 2015
Accepted 6 MAR 2016
Accepted article online 11 MAR 2016
Published online 8 APR 2016

1. Introduction

Oceanographic processes active in the Greenland Sea and in the Arctic Ocean (Figure 1) are important for the large scale circulation. The North Atlantic Current transports about 7.4 ± 1.1 Sv (1 Sv = 10^6 m^3/s) of warm and saline Atlantic water (AW) across the Greenland-Scotland Ridge, and some over continental shelf areas into the Nordic Seas (Greenland, Iceland, and Norwegian Seas) [*Hansen et al.*, 2015]. While part of the AW remains and participates in the processes in the Nordic Seas [e.g., *Swift and Aagaard*, 1981], a part flows to the Arctic Ocean through the Barents Sea [e.g., *Rudels*, 1986; *Blindheim*, 1989; *Ingvaldsen et al.*, 2004] and in the West Spitsbergen Current (WSC) through the Fram Strait [e.g., *Rudels*, 1987], where part of the northward flowing AW recirculates southwestward [e.g., *Bourke et al.*, 1988]. Warm, subsurface AW was observed in the Arctic Basin already by *Nansen* [1902] and the return flow of warm AW was observed in the East Greenland Current in the Fram Strait by *Ryder* [1891]. At the surface cold and low-saline surface water from the Arctic Ocean flows through the Fram Strait in the East Greenland Current (EGC) to the Greenland Sea and southward [e.g., *Manley*, 1995; *Fahrbach et al.*, 2001; *Rudels et al.*, 2005]. The deep water exchanges between the Arctic Ocean and the rest of the oceans are possible only through the 2600 m deep Fram Strait.

Cooling and sinking of the warm AW in the Nordic Seas is part of the thermohaline overturning circulation renewing and ventilating the deep waters in the oceans [*Rahmstorf*, 1995]. Southward flowing dense water crosses the Greenland-Scotland Ridge at several places, the most prominent being the Denmark Strait in the west and the Faroe Bank Channel in the east. The source for the Denmark Strait overflow water was initially proposed to be the intermediate water formed in the Iceland Sea [*Swift et al.*, 1980; *Swift and Aagaard*, 1981] but later also the Greenland Sea was considered to be a source for the denser part of the Denmark Strait overflow [*Smethie and Swift*, 1989]. Deep water from the Norwegian Sea, formed by mixing between the Greenland Sea and Arctic Ocean deep water [*Aagaard et al.*, 1985; *Rudels*, 1986; *Swift and Koltermann*, 1988], was considered to supply the overflow in the Faroe Bank Channel [*Dooley and Meincke*, 1981; *Borenäs and Lundberg*, 1988]. The processes in the basins of the Nordic Seas became regarded as major sources for the overflow water and thus drivers for the thermohaline overturning circulation in the Atlantic Ocean

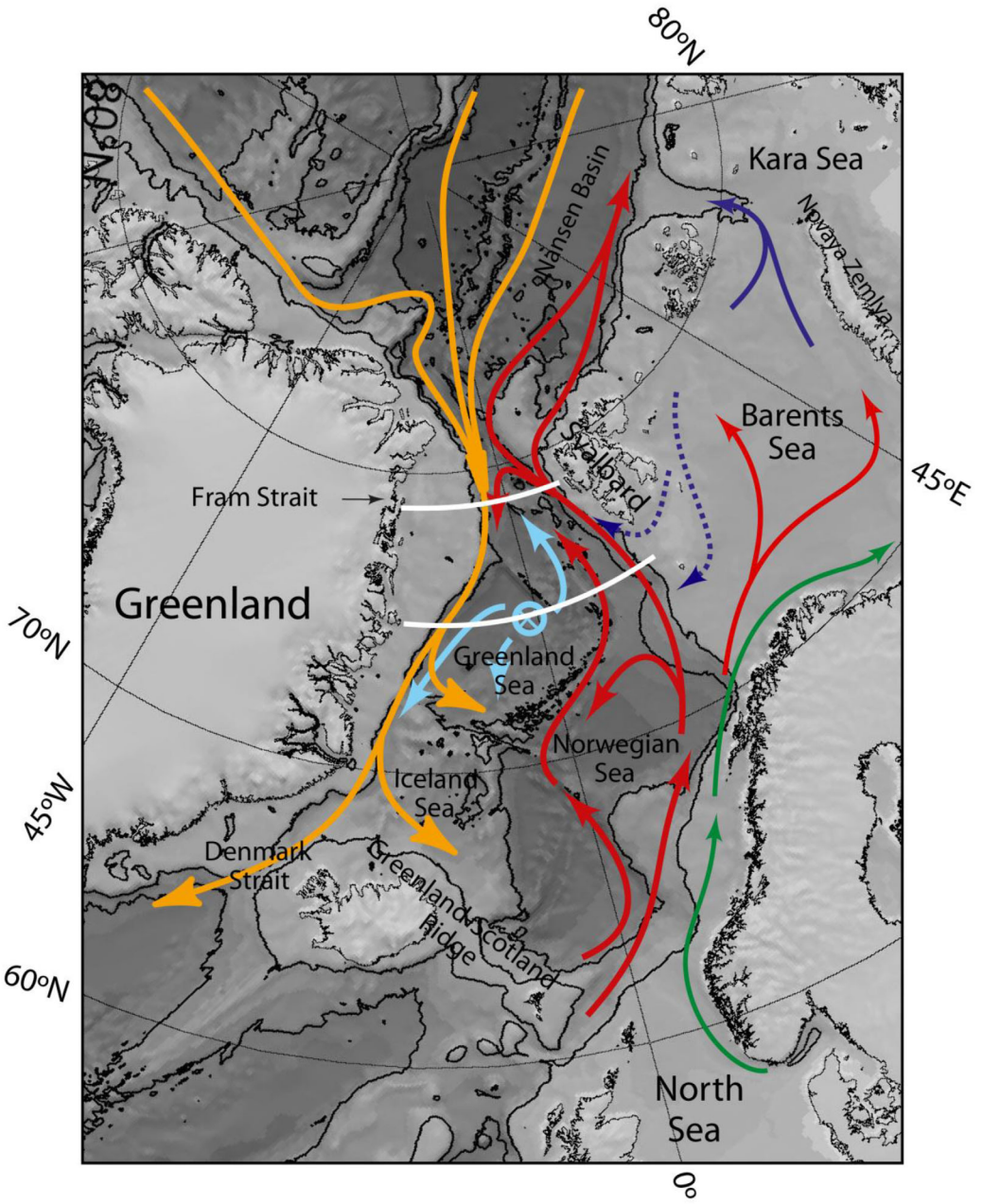

Figure 1. Locations of the 79°N and 75°N hydrographíc sections, and the Nordic Seas currents. Currents transporting AW (red), return AW (orange), Norwegian Coastal Current (green), and the Greenland Sea convective gyre waters (cyan).

(a detailed review provided by *Hansen and Østerhus* [2000]), and the convection in the Greenland Sea was considered as the main process.

No convection events reaching to the bottom in the Greenland Sea or the subsequent deep and bottom water renewal were documented in the Greenland Sea Project started in the 1980s, nor in the following experiments, and tracer studies indicated a reduced ventilation of the deep water after the 1970s [*Bönisch and Schlosser*, 1995]. In the 1990s, the temperature-salinity structure of the Greenland Sea water column started to change. An intermediate depth temperature maximum started to evolve and the doming of the isopycnals began to weaken. A likely explanation is that the deep convection was reduced and the dense bottom water was no longer renewed. This would have allowed for the less dense and warmer Amerasian (Canadian) Basin deep water, which before had been forced to continue along the Greenland slope toward the Iceland Sea and Denmark Strait, to penetrate

from the rim into the central Greenland Sea gyre [*Rudels*, 1995]. The intermediate water formed in the Greenland Sea became less dense and no longer sank deep enough to remove the intermediate temperature maximum. The convection in the Greenland Sea became limited to the layers above the intermediate temperature maximum, which was gradually displaced downward from 800 to 2000 dbar [*Budéus et al*., 1998; *Budéus and Ronski*, 2009]. In an earlier paper, *Quadfasel and Meincke* [1987] state that in some years convection does not extend below a few hundred meters so similar features may have existed before the 1990s.

The effects of the weakening deep convection on the overflow and the thermohaline overturning circulation were in the 1990s considered with some alarm and *Rahmstorf* [1995] pointed out that the increase in freshwater content in the upper layer might limit the dense water formation and result in a breakdown of the overturning circulation and thus a change to a weaker estuarine circulation as proposed by *Stommel* [1961]. However, at about the same time the importance of the dense water formations in the Greenland Sea and Iceland Sea gyres for the overflow and the thermohaline circulation became questioned. *Mauritzen* [1996a, 1996b] noted that the main increase in density of the Atlantic water entering the Arctic Mediterranean across the Greenland-Scotland Ridge occurs in the Norwegian Sea, and proposed that the Atlantic water that recirculates in the Fram Strait as well as the part that enters the Arctic Ocean and later returns in the East Greenland Current, were both already in the Fram Strait dense enough to supply the Denmark Strait overflow water. The formation of dense water in the deep basin gyres, by contrast, was regarded to be less important. This view of the origin of the Denmark Strait overflow water is still partly valid but has been modified since the discovery of the North Iceland Jet, which supplies the densest Denmark Strait overflow water from the Iceland slope [*Jonsson and Valdimarsson*, 2004].

At present, the Greenland Sea produces intermediate water with densities such that the water formed in the Greenland Sea can now contribute more directly to the overflow than earlier, when the water was too dense to cross the Greenland-Scotland Ridge. The Arctic Ocean deep waters that earlier were observed in the Denmark Strait [*Buch et al*., 1996], and perhaps also present north of the Iceland continental slope [*Rudels et al*., 1999], now penetrate into the Greenland Sea gyre and replace and transform, by mixing, the deeper layers in the Greenland Sea [*Meincke et al*., 1997; *Somavilla et al*. 2013]. This not only affects the Greenland Sea but also the deep waters advected from the Greenland Sea to the Fram Strait and into the Arctic Ocean. Some of these changes in the deeper layers occurring in the Fram Strait and in the Greenland Sea during the last 20 years have been reported [*Budéus and Ronski*, 2009; *Rudels*, 2010; *Langehaug and Falck*, 2012; *Rudels et al*, 2012; *von Appen et al*., 2015; *Wang et al*., 2015].

In this paper, the water mass properties and their changes are studied in the Fram Strait and in the Greenland Sea, and the transport of Arctic Ocean waters to the Nordic Seas, as well as the amount of waters transported to the Arctic Ocean through the Fram Strait, are estimated. Hydrographic sections from 1999 to 2010 in the Fram Strait and along 75°N in the Greenland Sea, reaching from the Greenland shelf to the Svalbard continental slope and the Barents Sea shelf, are combined to form a quasiclosed box. The oceanic transports of waters flowing through a box limited by the two sections are estimated from geostrophy and constrained by continuity requirements on volume and salt for different parts of the box. The effect of convection at the 75°N section is considered when defining the constraints. The velocities at 75°N are additionally constrained by advection velocities derived from Argo floats circulating in the Greenland Sea gyre. This work is an extension of the approach used by *Houssais et al*. [1995] and *Marnela et al*. [2013]. In section 2, the data used are described. In section 3, the method is described and the transports through the Fram Strait and the 75°N section are derived. In section 4, the mixing and water mass transformation in the Greenland Sea are examined and changes of water mass properties in the Greenland Sea and the Fram Strait are described. Section 5 contains the summary and discussion.

2. Data

Hydrographic sections have been obtained in 1999–2002, 2004, 2005, 2008, and 2010 through various projects, by mainly the Alfred Wegener Institute's (AWI) research vessel Polarstern, and the 2000 Fram Strait section by the Norwegian Polar Institute's (NPI) research vessel Lance, with one section located at 75°N crossing the Greenland Sea and the other in the Fram Strait at approximately 79°N (78° 49′N to 79° 10′N) so that both sections reach from the western to eastern shelf (Table A1a). The instruments used were SBE 911+ CTD (Conductivity, Temperature, Depth) profilers.

The data have been averaged for every 1 dbar except for the 1999 Fram Strait data which have been averaged to 2 dbar intervals, thus for the corresponding 75°N section in 1999 every second value is used.

Salinity spikes greater than 0.003 have been removed from the data. Gaps in the vertical have been linearly interpolated over. Missing 2–4 m at the surface have been extrapolated to the surface using the uppermost observation of the cast as a constant value. Instabilities are unremoved and unsmoothed.

At the 75°N section coherent vortices, long-lived regions of swirling flow [*Gascard et al*., 2002; *Oliver et al*., 2008], can be present. Temperatures and salinities in these vortices differ from the surroundings and thus affect the mean temperatures and salinities averaged for the sections as noted by *Budéus and Ronski* [2009]. Coherent vortices have been removed from the Greenland Sea deep basin in 2001 (one station) and 2002 (four stations).

Historical temperature and salinity data from the Greenland Sea from the late 1970s onward as well as newer data from the Greenland and Norwegian Seas and the Fram Strait (Table A1b) are used to provide supplementary information about the changes in the water mass properties.

Argo floats provide year-round profiles from the Nordic Seas as well as an estimate for the drift. Argo floats usually follow the currents at a fixed pressure and take a temperature and salinity profile every 10 days between a maximum depth of 2000 dbar and the surface. Most of the floats used in this study had a parking depth of 1000 dbar, but some had a parking depth of 500 or 1500 dbar. Argo data are collected and made freely available by the International Argo Program and the national initiatives that contribute to it (http://www.argo.net). Argo is a pilot program of the Global Ocean Observing System. Argo data for the Greenland Sea area are available online from 2001 onward and for the Fram Strait from 2006 onwards. For this study, quality-checked (Delayed Mode Quality Control - DMQC) Argo data not included in the grey list were downloaded from http://www.coriolis.eu.org which is one of the two Global Data Assembly Centers (GDACs).

3. Method

3.1. Transport Estimates

3.1.1. Geostrophic Method

Transports between the Nordic Seas and the Arctic Ocean are estimated from 8 years of hydrographic measurements between 1999 and 2010. Two hydrographic sections, one located at 75°N in the Greenland Sea and the other at approximately 79°N in the Fram Strait have previously been studied separately [e.g., *Budéus and Ronski*, 2009; *Langehaug and Falck*, 2012; *Somavilla et al*., 2013], and are now combined to form a quasiclosed box in a way similar to *Houssais et al*. [1995] and *Marnela et al*. [2013]. All water exchange between the Fram Strait and the Nordic Seas is assumed to pass through the two sections. Geostrophic transports are computed setting the velocity to zero near the bottom. The stations are not of equal depth and the method of *Jacobsen and Jensen* [1926] is used to estimate velocities for the deeper station in a station pair, below the common depth of the two stations that the geostrophic velocity is computed between. See Marnela et al. [2013] for details.

3.1.2. Conservation Constraints

Four conservation constraints are applied requiring a balance between the net transports consisting of the transports carried by the baroclinic part of velocities obtained from the geostrophic computations and by the unknown barotropic part of the velocities. The constraints are set in a method similar to that described in *Houssais et al*. [1995] and *Marnela et al*. [2013] and are:

$$\iint_{\gamma 1} v^b(x)S(x,z)dxdz = C_1 - \iint_{\gamma 1} v^{bc}(x,z)S(x,z)dxdz \tag{1}$$

$$\iint_{\gamma 2} v^b(x)dxdz = C_2 - \iint_{\gamma 2} v^{bc}(x,z)dxdz \tag{2}$$

$$\iint_{\gamma 2} v^b(x)S(x,z)dxdz = C_3 - \iint_{\gamma 2} v^{bc}(x,z)S(x,z)dxdz \tag{3}$$

$$\iint_{\gamma 3} v^b(x)dxdz = C_4 - \iint_{\gamma 3} v^{bc}(x,z)dxdz, \tag{4}$$

where $v^b(x)$ is the depth-independent barotropic velocity to be determined, $v^{bc}(x,z)$ is the baroclinic velocity, S is salinity × density and γ_k (k = 1,. . .,4) stands for the area of the CTD sections over which the

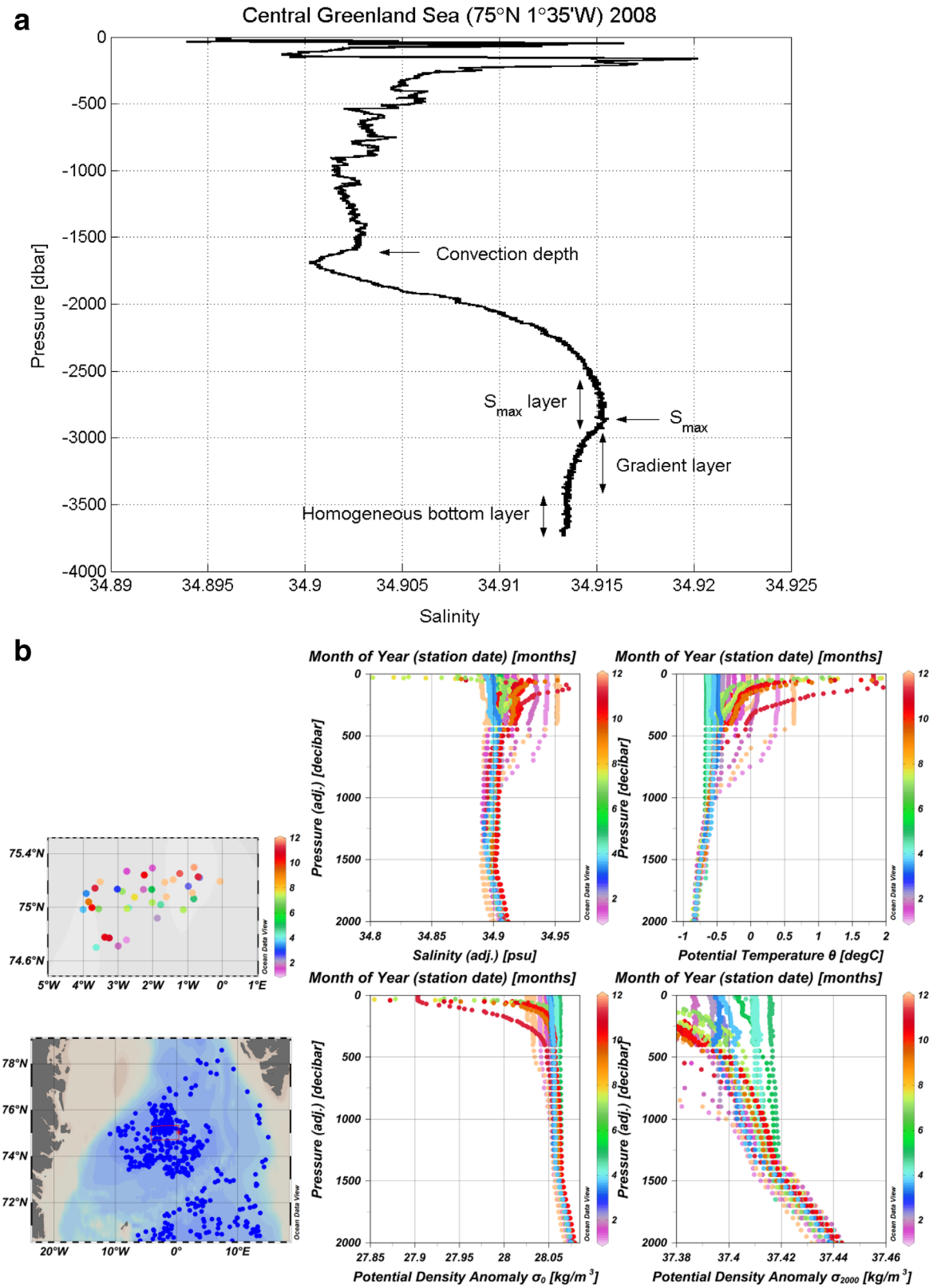

Figure 2. (a) A salinity profile from the central Greenland Sea in 2008 with the convection depth, salinity maximum, salinity maximum layer, gradient layer, and the homogeneous bottom layer marked with arrows. (b) The seasonal cycle (from November 2007 to October 2008) in the central Greenland Sea as observed in the potential temperature and salinity profiles obtained from Argo floats. The month of observation is shown in color in the profiles and on the map.

Table 1. Convection Depths Estimated From Hydrography (CTD, and Argo Floats When Available) in the Greenland Sea at About 75 ± 0.5°N and Between 5°W and 1°E, and the Salinity and Potential Temperature at the Bottom From 1999 to 2013[a]

Year	Convection Depth (dbar)	Convection Depth From Literature (dbar)	S Bottom	θ Bottom (°C)
1999	700	700 (BR)	34.902	−1.16
2000	1400	1400 (BR)	34.902	−1.14
2001	1400–2000	1400 (BR)	34.903	−1.13
2002	1600–2500	1600 (BR), 1100 (LQ), 1500 (L)	34.905	−1.11
2003	200	1600 (BR), 200 (LQ, L)	34.906	−1.10
2004	800	1000 (BR)	34.907	−1.09
2005	700	800 (BR) 600 (LQ, L)	34.908	−1.07
2006	800	800 (LQ), 1200 (L)	34.9095	−1.06
2007		600 (LQ), 1400 (L)	34.911	−1.05
2008	1700	1500 (M), 1800 (L)	34.9125	−1.03
2009	700–1800	1700 (L)	34.9135	−1.01
2010	200	400 (L)	34.914	−1.00
2011	1900	1900 (L)	>34.915	<−0.97
2012	400	300 (M)	>34.916	<−0.96
2013	1500		34.918	−0.96

[a]The 2011 and 2012 values are estimated from shallower CTD data by adding 0.002 to salinity and subtracting 0.02°C from potential temperature based on differences in the temperature and salinity profiles during the other years. The 2011 and 2012 CTD data are not from the center of the GS gyre and the actual values inside the gyre may be slightly colder and more saline. A range is given when coherent vortices are present (2001, 2002) or when distinguishing whether the maximum observed convection depth originates from an earlier year (2009). The values obtained by other studies are presented: *Ronski and Budéus* [2005] *Budéus and Ronski* [2009] (BR), *Latarius and Quadfasel's* [2010] (LQ), *Latarius* [2013] (L), and *Moore et al.* [2015] (M).

constraint is applied. The boxes are assumed to have no sources and sinks and the constraints C_k are equal to zero.

Salt balance is required for the whole area (constraint 1). Two additional constraints require a balance of volume (2) and salt (3) transports between an estimated maximum depth of the Greenland Sea convection during the 1999–2010 observation period, 1900 dbar, and the Fram Strait sill depth (Figure 2 and Table 1). The upper limit is kept constant at 1900 dbar due to difficulty in annually estimating the convection depth with certainty, and to avoid the influence of upper ocean processes during years of shallow convection. In 2001 and 2002, coherent vortices are found in the GS section that reach deeper than 1900 dbar, in 2001 to about 2000 dbar, and in 2002 to 2500 dbar. These vortices are removed and their effect assumed local. The sill depth is at about 2600 dbar [Klenke and Schenke, 2002], but since the deepest Fram Strait stations reach below 2700 dbar, 2700 dbar is used as the lower limit. A volume balance is also required for the deep Greenland Sea below 2700 dbar (constraint 4).

A variational approach is then used to find the least energetic barotropic corrections needed to fulfil the constraints in a way similar to the method in *Rudels et al.* [2008]. The barotropic velocity component v^b is computed by minimizing the kinetic energy of the barotropic part using the method of Lagrangian multipliers [*Lanczos*, 1970; *Wunsch*, 1978; *Stommel and Veronis*, 1981]. The barotropic reference velocities are determined by solving the Moore-Penrose inverse with no error term introduced in the equations. See details in Marnela et al. [2013].

3.1.3. Argo-Based Velocity Adjustment

In an extension to the approach, the drift estimated from Argo floats with parking depths at 1000 and 1500 dbar (Figure 3) is used to adjust the geostrophic velocities at the 75°N section. The difference between 1000 and 1500 dbar velocities was found small, under 0.3 cm/s in most of the Nordic Seas, by *Voet et al.* [2010] and velocities at both pressures are considered representative of the velocity at 1000 dbar. Argo velocities are estimated from two consequent surface observations: from the last location before the dive and the first location after the dive. Thus derived velocities are assigned a location halfway between the two observations. *Voet et al.* [2010] provide a detailed analysis of the errors involved in the velocity estimation from the Argo floats, e.g., about the actual route of the float versus a straight line estimate, and the

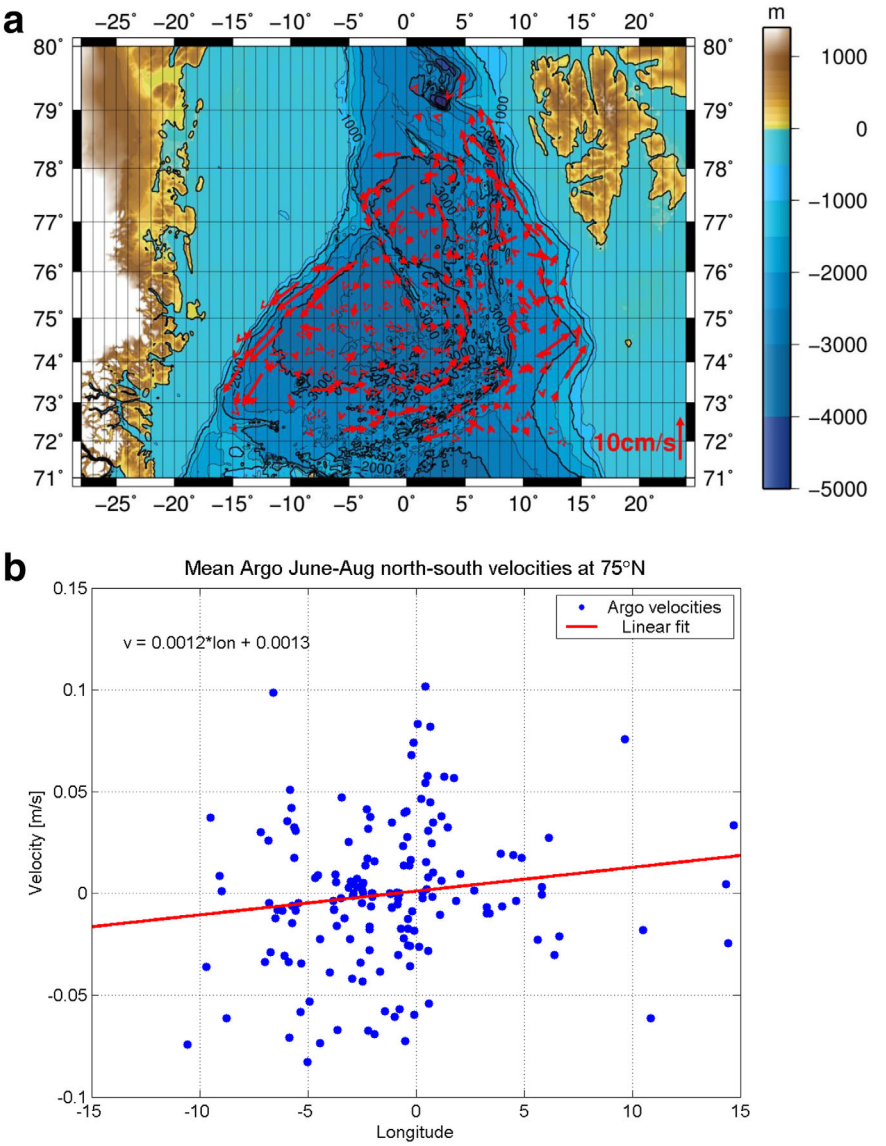

Figure 3. (a) Velocities averaged from June to August Argo float data in 2001–2010 at 1000 and 1500 dbar. Map produced with GMT [*Wessel and Smith*, 1998]. (b) Argo derived northward-southward velocities (m/s) from June to August 2001–2010 with a linear fit. Velocities in northward direction are positive and in southward negative.

inaccuracy of the surface positioning system. A seasonal minimum in the velocities during summer is noted by *Voet et al.* [2010], which is when the hydrographic data have been collected. Argo summer data (June–August) between years 2001 and 2010 from within ±0.5 degree of the 75°N latitude are thus selected for adjusting the geostrophic velocities. The north-south components corresponding to the directions of geostrophic velocities across the zonal Greenland Sea section are shown in Figure 3b. For example, *Voet et al.* [2010] describe a cyclonic flow along the rims of the Greenland Sea basin. The Argo velocities tend to be highest at the rims of the Greenland Sea gyre, at 75°N the velocities estimated from the drift of the floats are on the rims as high as 20 cm/s at 500 and 1000 dbar levels, and above 10 cm/s during summer (Figure 3, only velocities at 1000 and 1500 dbar are shown) and in the center close to zero or variable. At about 79°N the maximum velocities from the floats drifting at 1000 dbar are about 10 cm/s.

A linear fit is applied to the Argo derived north-south velocity components from the GS section between 12.5°W and 15°E, i.e., for the section part deeper than the parking depth of the Argo floats (1000 dbar). The linear fit gives 0.0012 m/s × longitude + 0.0013 m/s. In order to not add a net transport to the section based on this simple approximation, the slope of the linear fit is kept but a new constant term is found

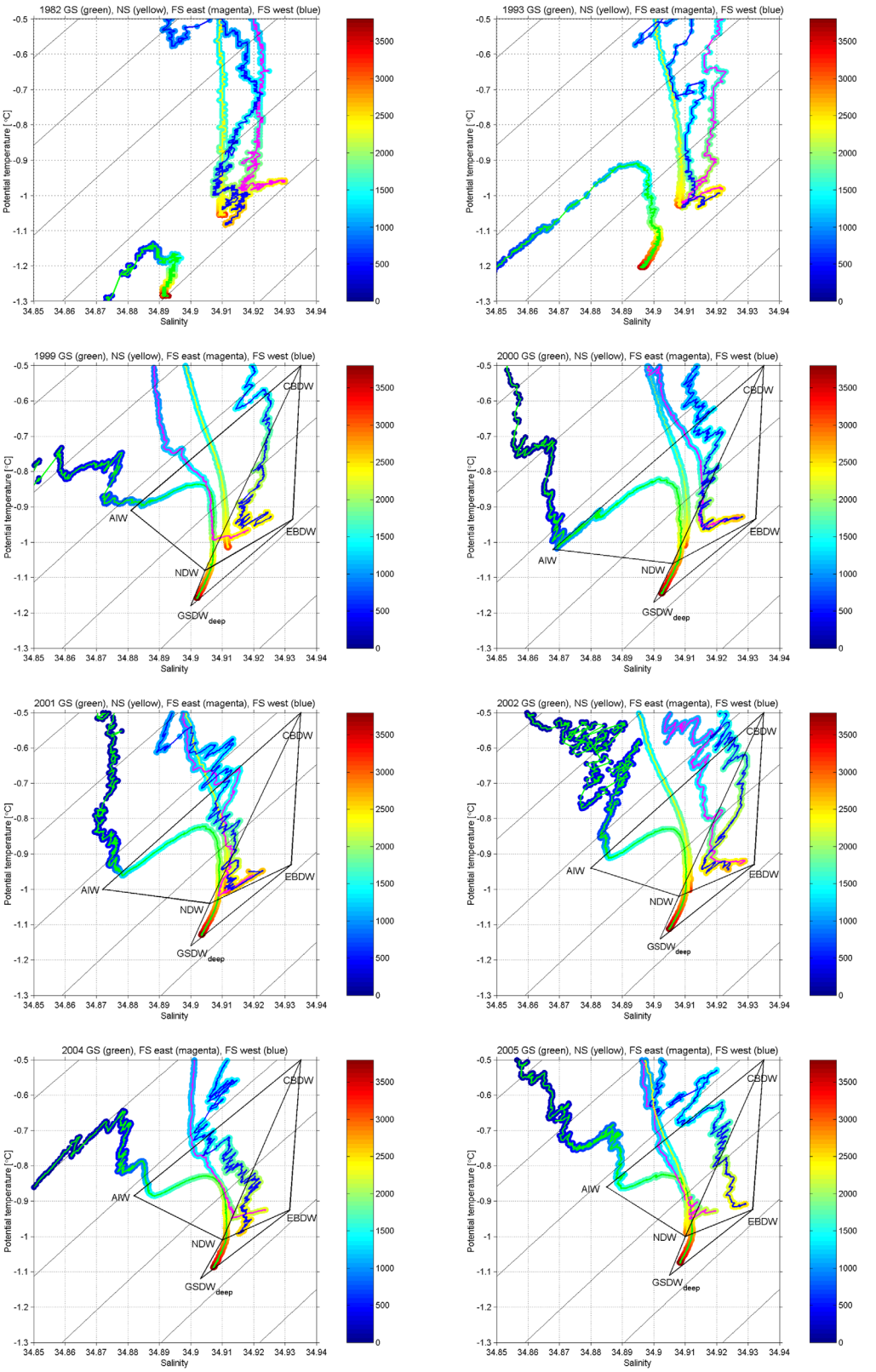

Figure 4. Potential temperature-salinity diagrams with waters from the Greenland Sea (GS), Norwegian Sea (NS), and Fram Strait (FS west and FS east) from 1982 to 2013 showing how the differences in the deep waters have become smaller. Pressure values are indicated with colour. Potential density at 2000 dbar isolines from 37.375 to 37.5 kgm^{-3} are shown. Water mass triangles with annually varying vertices (water mass end-members) are shown. Map with the locations of the station profiles is produced with GMT [*Wessel and Smith*, 1998].

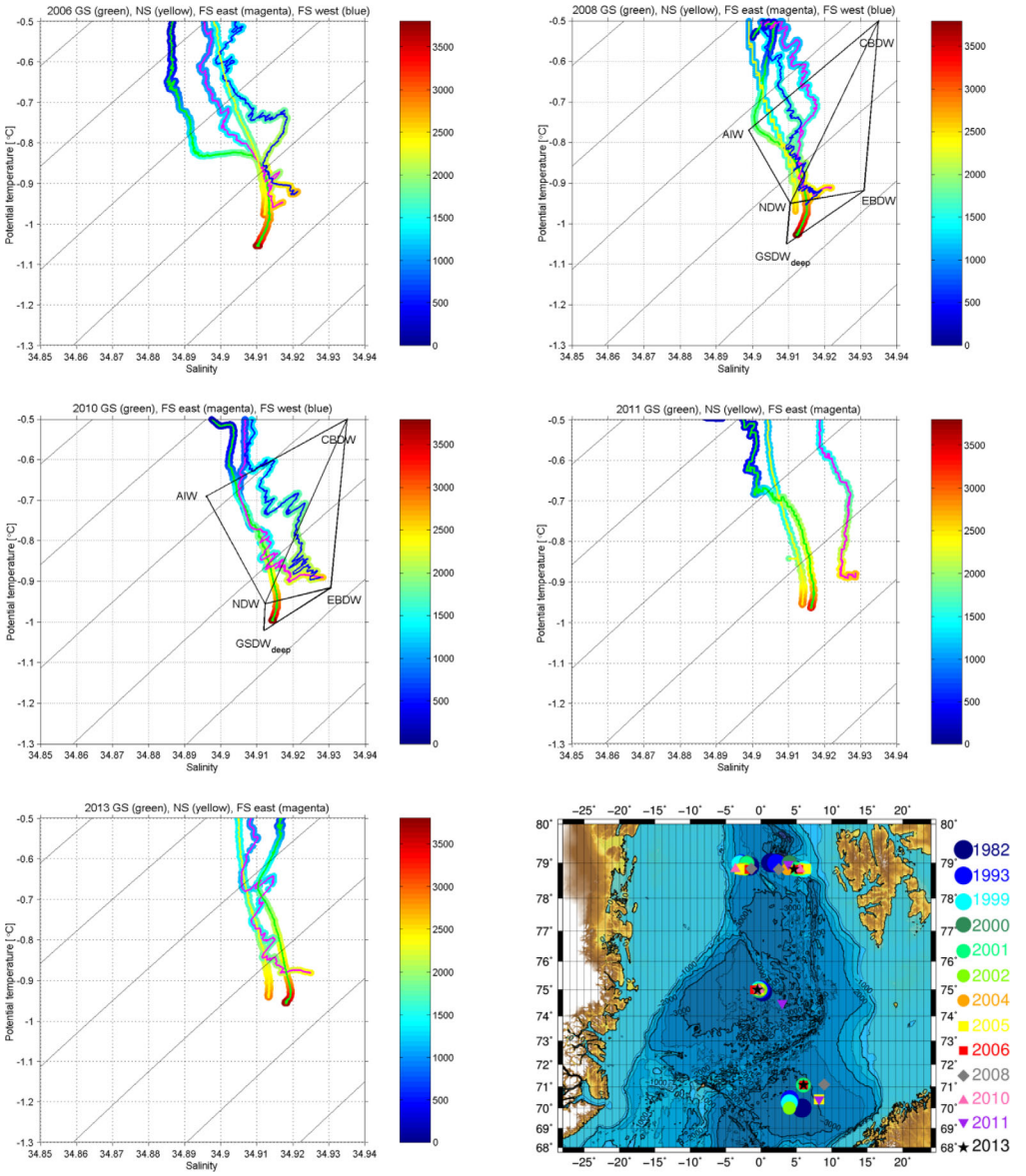

Figure 4. (continued)

annually that balances with area (the bottom description varies slightly depending on where the stations are located). The constant term added to 0.0012 m/s × longitude varies between −0.00069 and −0.00039 m/s. The function gives a velocity at 1000 dbar for the deep part of the GS section that is northward in the east and southward in the west and one order of magnitude smaller than the maximum velocities obtained from the Argo floats. This velocity is assumed to be absolute and the difference between this Argo linear fit velocity and the geostrophic velocity at 1000 dbar is then added as a constant to the geostrophic velocities of the whole water column. The four constraints used in the first approach are then applied.

3.2. Water Mass Transports and Changes

The water masses in the Greenland Sea and in the Fram Strait are first separated into six water mass classes based mainly on densities (Table A2): (1) Surface water, (2) Atlantic Water (AW), (3) dense AW (dAW), (4) intermediate water, (5) deep water I including Canadian Basin Deep Water (CBDW) and the lightest part of the Nordic Seas Deep Water (NDW), and (6) deep water II including Eurasian Basin Deep Water (EBDW) and the deeper part of the Nordic Seas Deep Water (NDW) following the definition by *Rudels et al.* [2005] and *Rudels et al.* [2008]. However, changes in the Greenland Sea deep water mass properties, i.e., warming

Table 2. Net Volume Transports (Sv) From Geostrophy With (a) Four Constraints Applied, (b) With Argo Adjustment First and Then Four Constraints Applied[a]

a)

Year	75°N Northward	75°N Southward	75°N Net	79°N Northward	79°N Southward	79°N Net
1999	13.5	−14.5	−1.0	6.9	−7.9	−1.0
2000	17.9	−18.7	−0.8	6.8	−7.6	−0.8
2001	14.7	−15.7	−0.9	11.2	−12.2	−1.0
2002	14.0	−17.0	−3.0	10.2	−13.1	−3.0
2004	14.2	−16.0	−1.7	8.1	−9.9	−1.8
2005	16.5	−18.8	−2.3	7.2	−9.5	−2.4
2008	11.3	−14.6	−3.3	8.4	−11.8	−3.4
2010	11.9	−14.3	−2.5	14.8	−17.3	−2.5
MEAN	14.3	−16.2	−1.9	9.2	−11.2	−2.0
STD	2.2	1.8	1.0	2.8	3.2	1.0

b)

1999	16.0	−16.0	−0.0	7.6	−7.7	−0.1
2000	18.7	−18.9	−0.3	7.3	−7.6	−0.3
2001	18.4	−16.0	2.4	13.0	−10.6	2.4
2002	14.3	−16.8	−2.6	10.7	−13.2	−2.5
2004	15.5	−16.8	−1.3	8.6	−9.9	−1.3
2005	18.2	−19.7	−1.6	7.5	−9.0	−1.6
2008	13.2	−14.7	−1.5	9.7	−11.2	−1.6
2010	14.8	−16.0	−1.2	15.6	−16.8	−1.2
MEAN	16.1	−16.9	−0.8	10.0	−10.8	−0.8
STD	2.1	1.7	1.5	3.0	3.0	1.5

[a]Coherent vortices have been removed from both for years 2001 and 2002.

and salinification [*Somavilla et al*., 2013], make it eventually impossible to distinguish between deep waters of the Arctic Ocean and of the Nordic Seas origin using a constant salinity like in for example, *Rudels et al*. [2005] (Figure 4) Also the Arctic Ocean water masses have become warmer, but not to the same degree [*Rudels et al*., 2013; *von Appen et al*., 2015]. The deep water masses are therefore redefined by forming a set of triangles where the vertices of the triangles represent potential temperature and salinity properties of

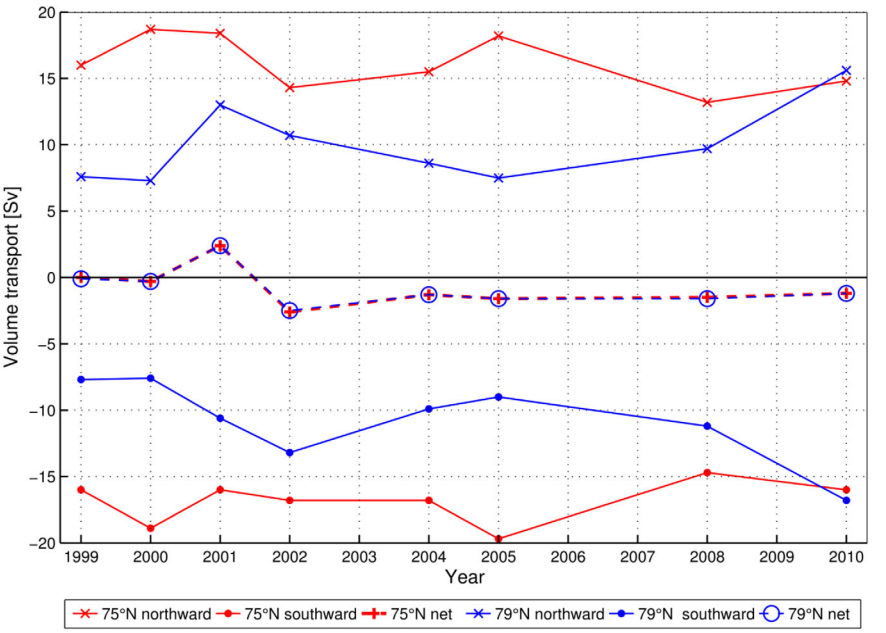

Figure 5. Northward, southward, and net volume transports (Sv) from geostrophy with Argo adjustment and four constraints applied. Coherent vortices have been removed in 2001 and 2002.

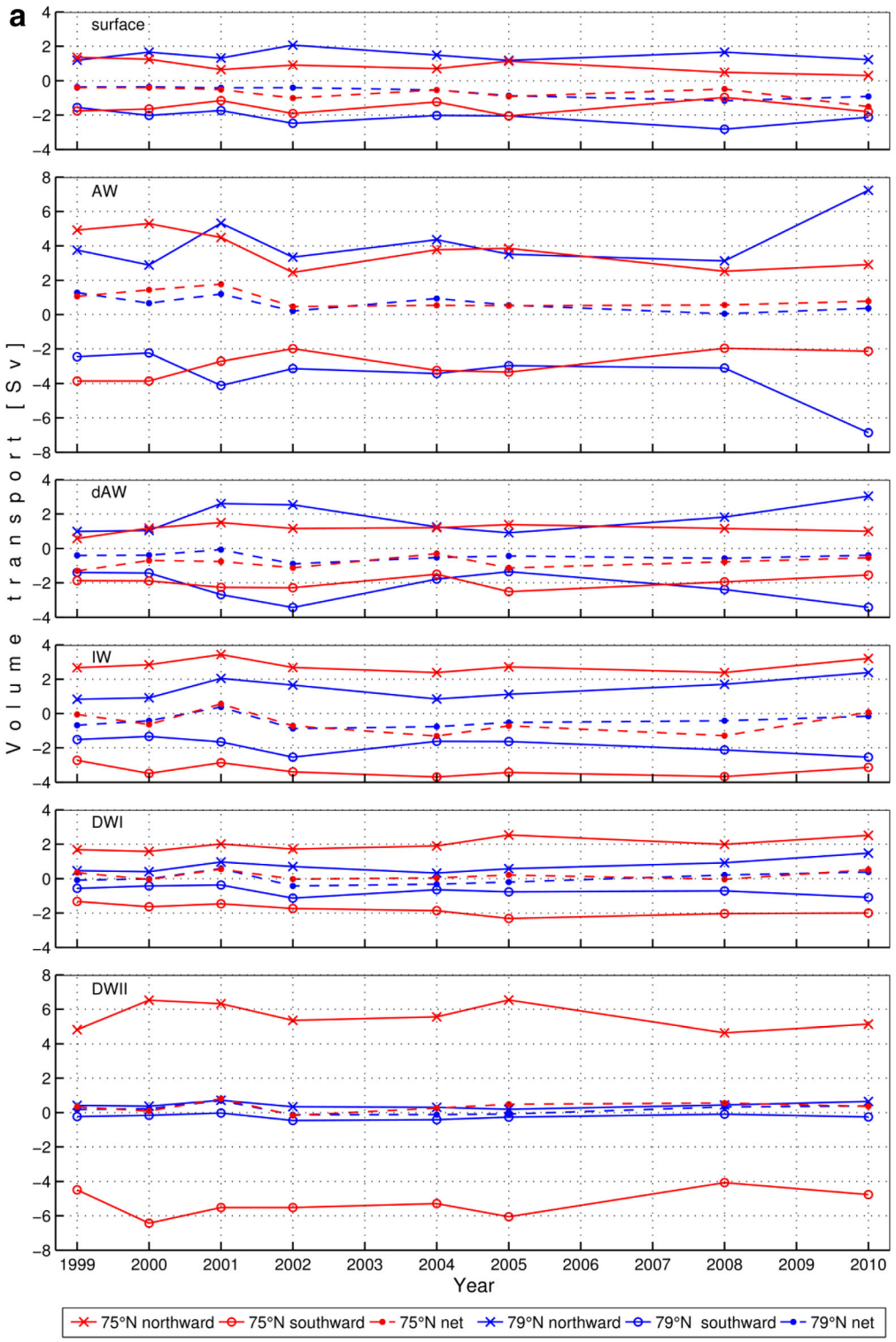

Figure 6. (a) Volume transports and properties of surface water, Atlantic waters, intermediate water, and deep waters following the water mass classification of *Rudels et al*. [2005, 2008] in FS and GS, with Argo adjustment and four constraints applied. Northward transports are positive and southward negative. (b) Intermediate and deep water volume transports (Sv) through FS and GS, with Argo adjustment and four constraints applied. Triangle division with annually varying vertices is used. Northward transports are positive and southward negative. (c) Intermediate and deep water volume transports (Sv) through FS and GS, with Argo adjustment and four constraints applied. Triangle division with fixed vertices, except AIW varying annually, is used. Northward transports are positive and southward negative.

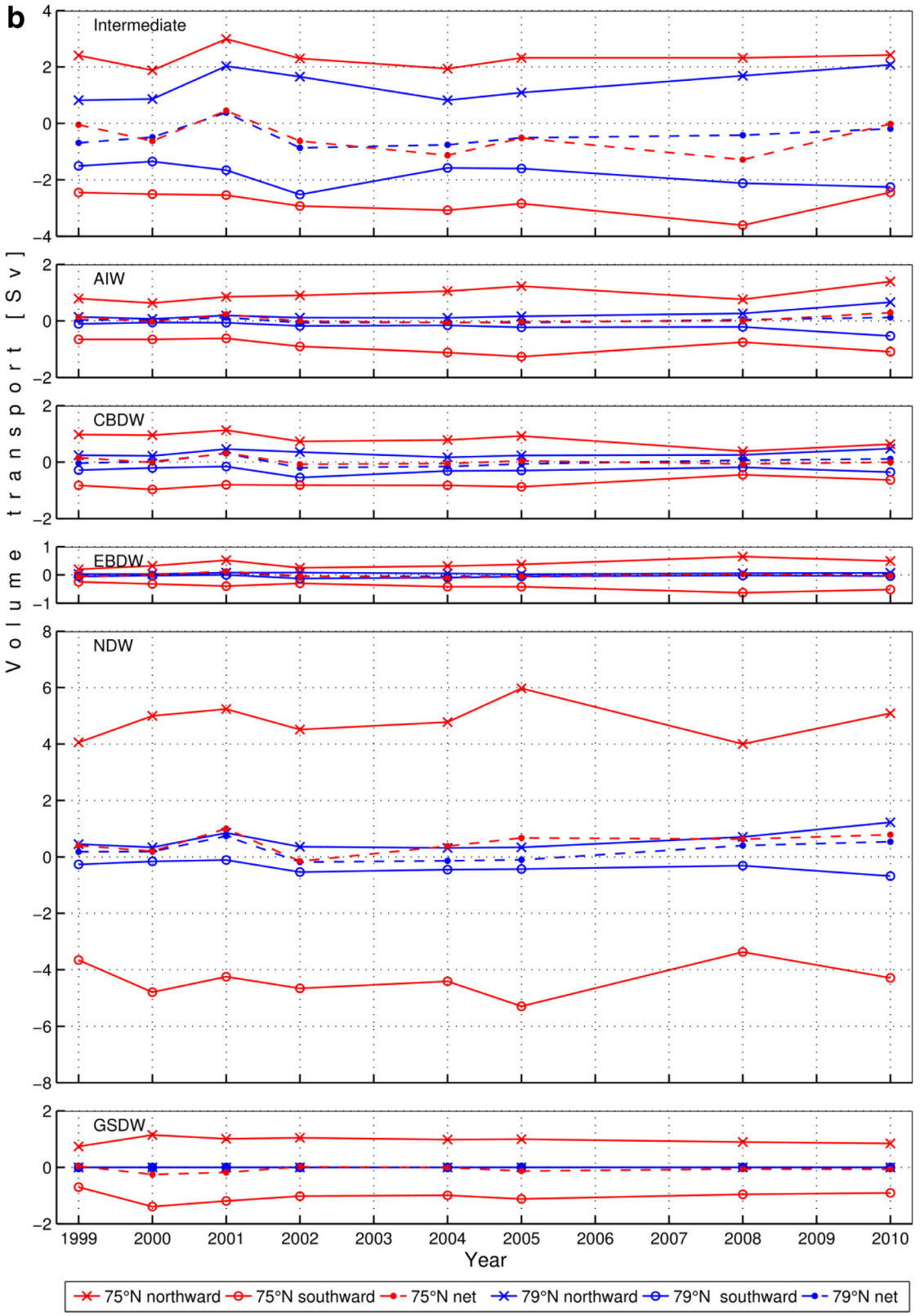

Figure 6. (continued)

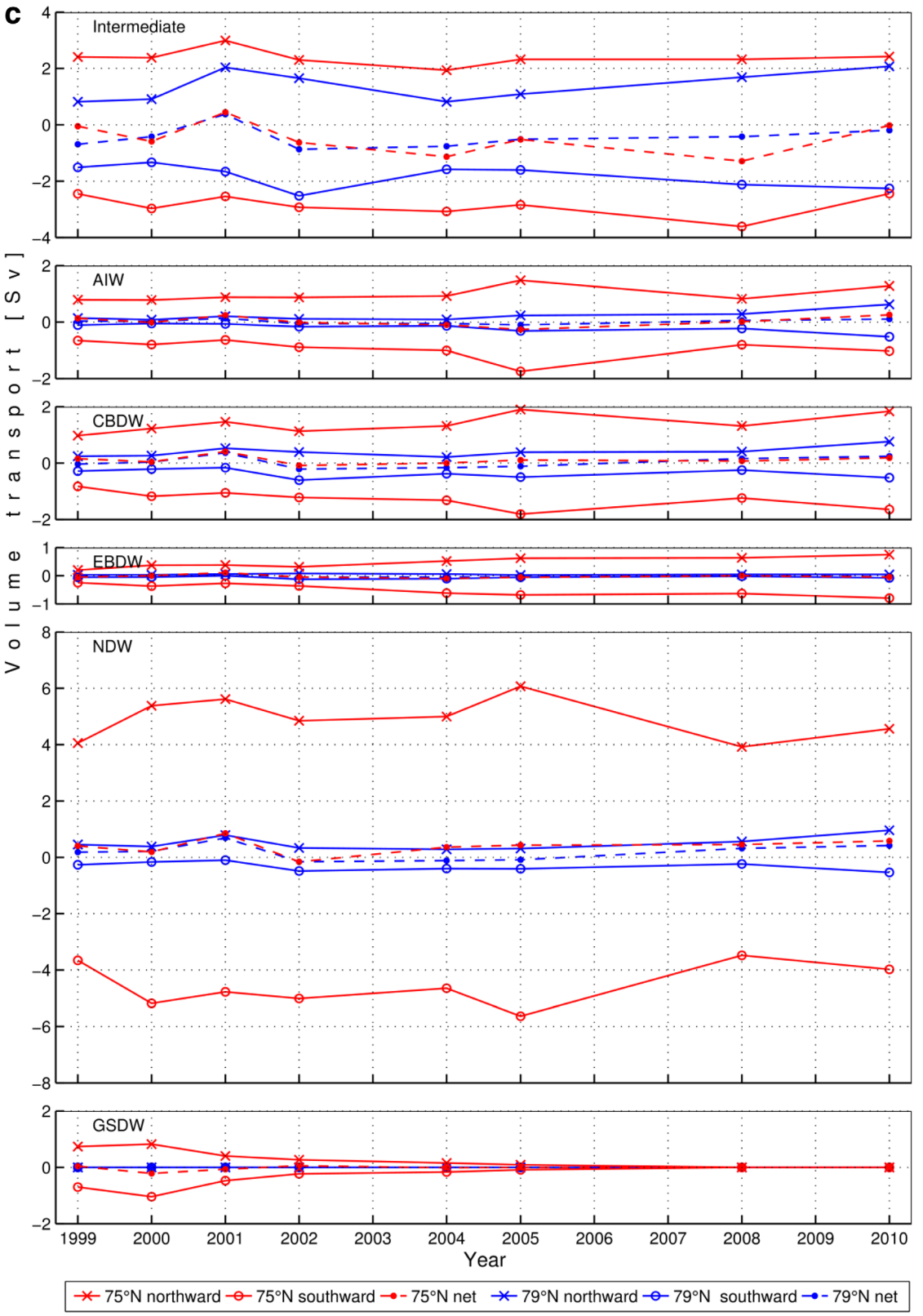

Figure 6. (continued)

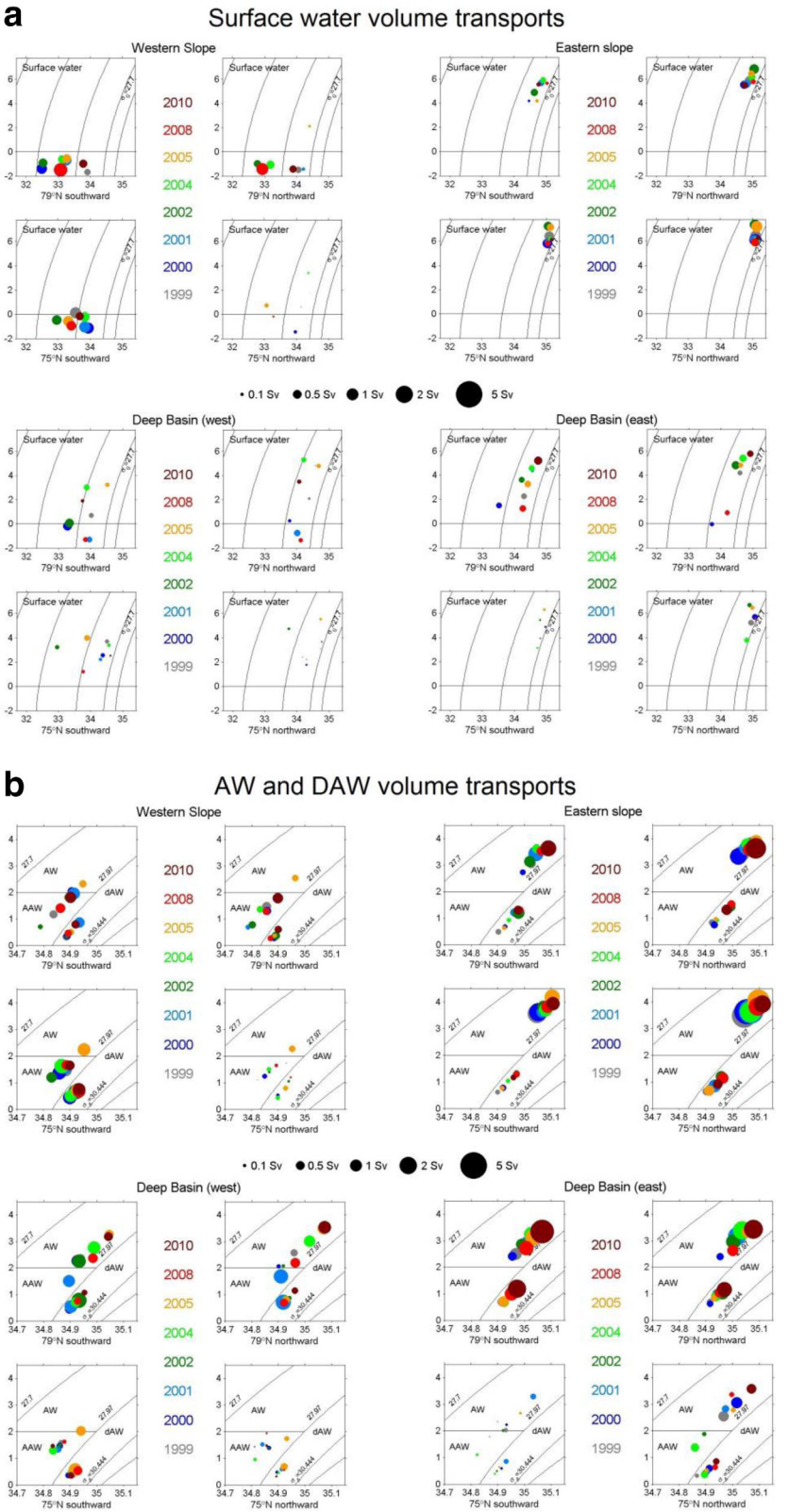

Figure 7. Potential temperature (*y* axis) and salinity (*x* axis) volume bubbles from six water mass classes [*Rudels et al.*, 2005, 2008] with Argo adjusted geostrophy and four constraints applied. Deep waters are separated in a dense and less dense part (DWI and DWII; (a)–(c)) or based on water mass triangles with annually varying vertices (d).

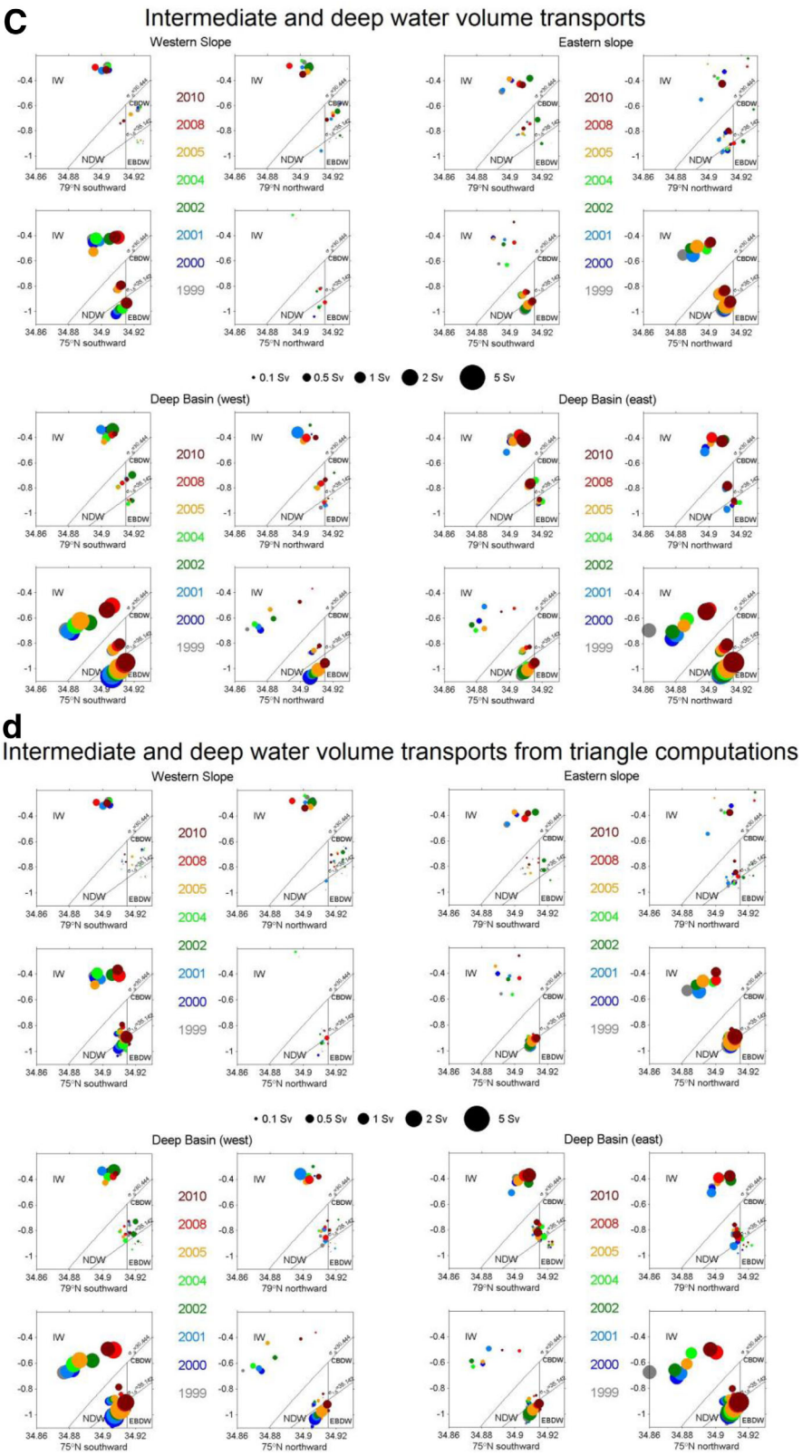

Figure 7. (continued)

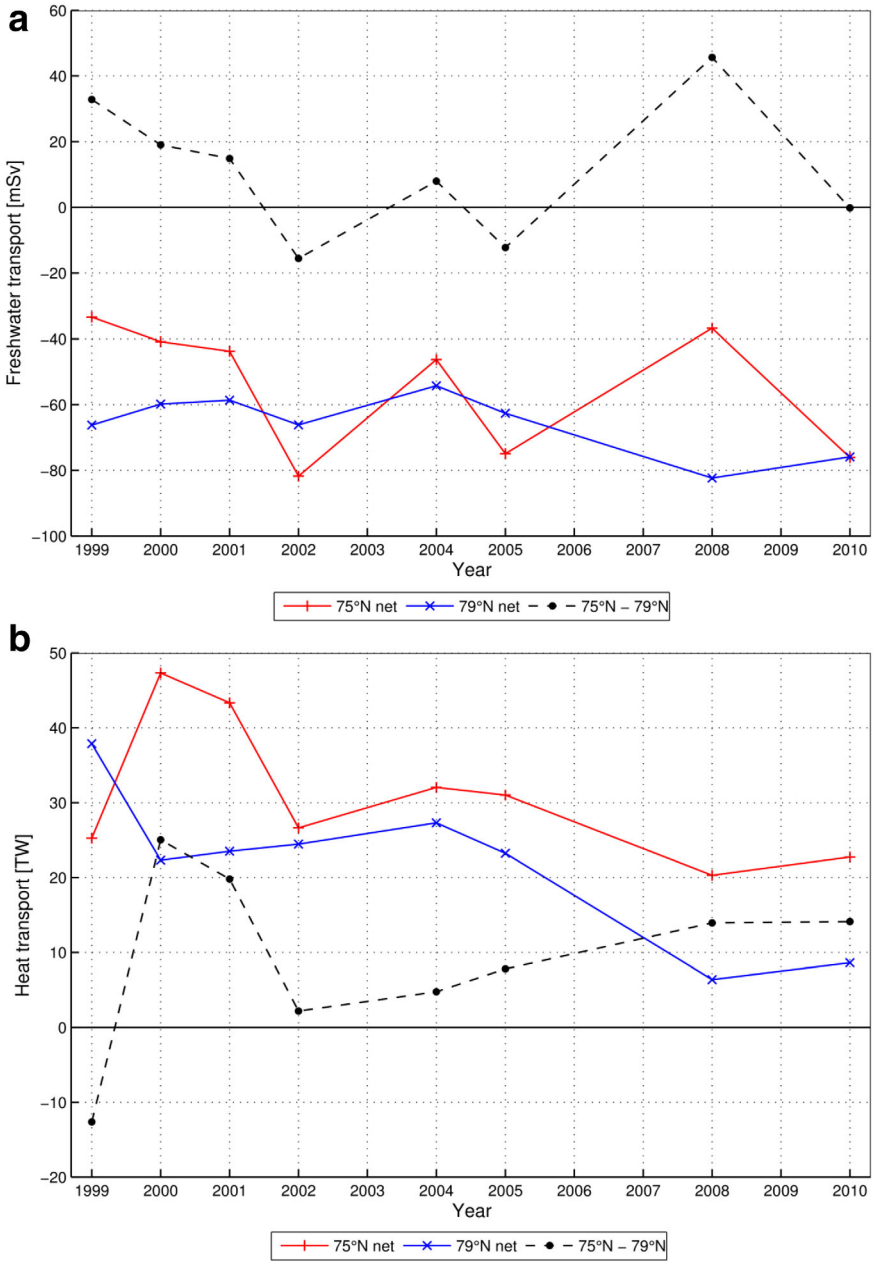

Figure 8. (a) Relative heat transports (relative to −0.1°C), and (b) liquid freshwater transports (mSv) (relative to 34.9) at the FS and GS sections. Northward transports are positive and southward negative. The subtraction between GS and FS sections (black lines) is the heat/freshwater divergence (negative) or convergence (positive) between the sections.

deep and intermediate water masses present in the Fram Strait and in the Nordic Seas (Figure 4). Water mass values inside the triangles can be thought to be a mixture of water mass properties found at the vertices of the triangle. The fractions f (from 0 to 1 inside the triangle) of each end point member of water can be found by solving a set of equations for each point i inside a triangle:

$$\begin{aligned} f_1 \cdot S_1 + f_2 \cdot S_2 + f_3 \cdot S_3 &= S_i \\ f_1 \cdot \theta_1 + f_2 \cdot \theta_2 + f_3 \cdot \theta_3 &= \theta_i \\ f_1 + f_2 + f_3 &= 1 \end{aligned} \tag{5}$$

Three triangles with the following vertices are formed: (1) AIW (Arctic Intermediate Water) – CBDW – NDW, (2) EBDW – NDW – CBDW, and (3) EBDW– $GSDW_{deep}$ – NDW (Figure 4). The end points are defined as: AIW

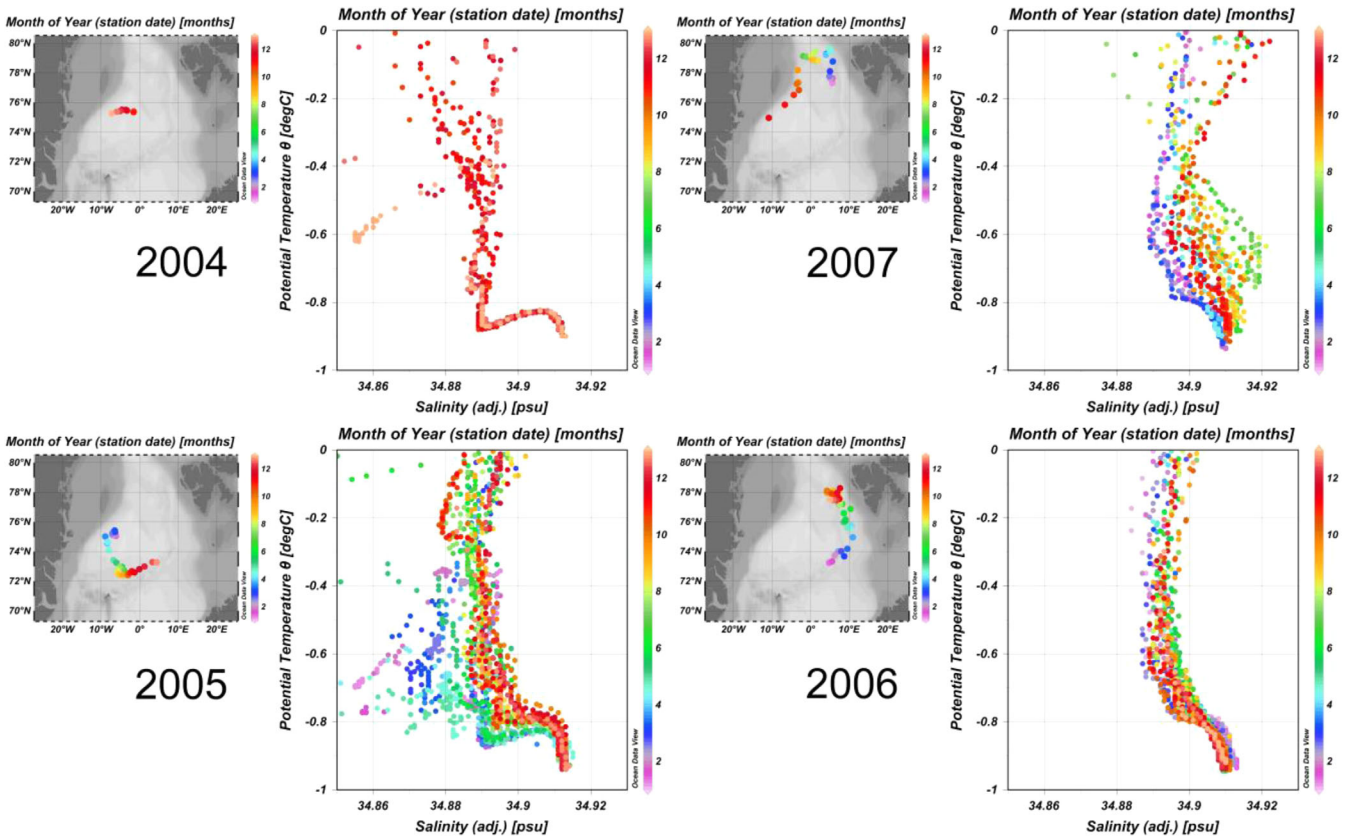

Figure 9. Argo float WMO# 6900303 in 2004–2007: Float surface locations on a map and θS diagrams showing the seasonal and spatial changes in temperature and salinity.

as present in the Greenland Sea, CBDW at the Lomonosov Ridge sill depth in the Canada Basin, EBDW as in the Nansen Basin at the Fram Strait sill depth, NDW in the Greenland Sea at the Fram Strait sill depth, and $GSDW_{deep}$ (Greenland Sea deep water closest to the bottom in the Greenland Sea). However, to fit in most data inside the triangles, the vertices of AIW, NDW, and $GSDW_{deep}$ need to be chosen slightly outside of the values present in the Greenland Sea. The values for AIW, NDW, and $GSDW_{deep}$ are allowed to vary annually and are estimated from hydrographic data. CBDW properties are kept constant. EBDW changes are small and estimated from sparse data using linear interpolation and when necessary slightly adjusted to fit data inside the triangles.

Surface water, AW and dAW are defined as previously [*Rudels et al*., 2008]. Not just the deep waters but also the intermediate waters are affected by the new definition. Instead of separating the intermediate and deep waters at a constant density, the annually changing line AIW–CBDW is chosen as the boundary between the intermediate and deep waters.

Transports through the FS and GS sections are computed for the six water masses in Table A2 from geostrophy with four constraints applied both without (Table 2, only transports for the whole water column are shown, not for the individual water mass classes) and with Argo adjustment (Table 2, Figures 5 and 6). Each of the two sections is further separated to 4–5 parts: deep basin split in two at the zero meridian, slopes on both sides and the EGC shelf when available (Figure 7). Transports from the Argo adjusted velocities are also computed based on the triangle water mass composition (Figures 6 and 7).

3.3. Mixing

Mixing is studied from the Greenland Sea hydrographic data collected between years 1977 and 2013 (earlier data exists, but the necessary features are difficult to extract due to few stations or vertically sparse data) using the method of *Meincke et al.* [1997]. The salinities (temperatures) are found at the deep salinity maximum and

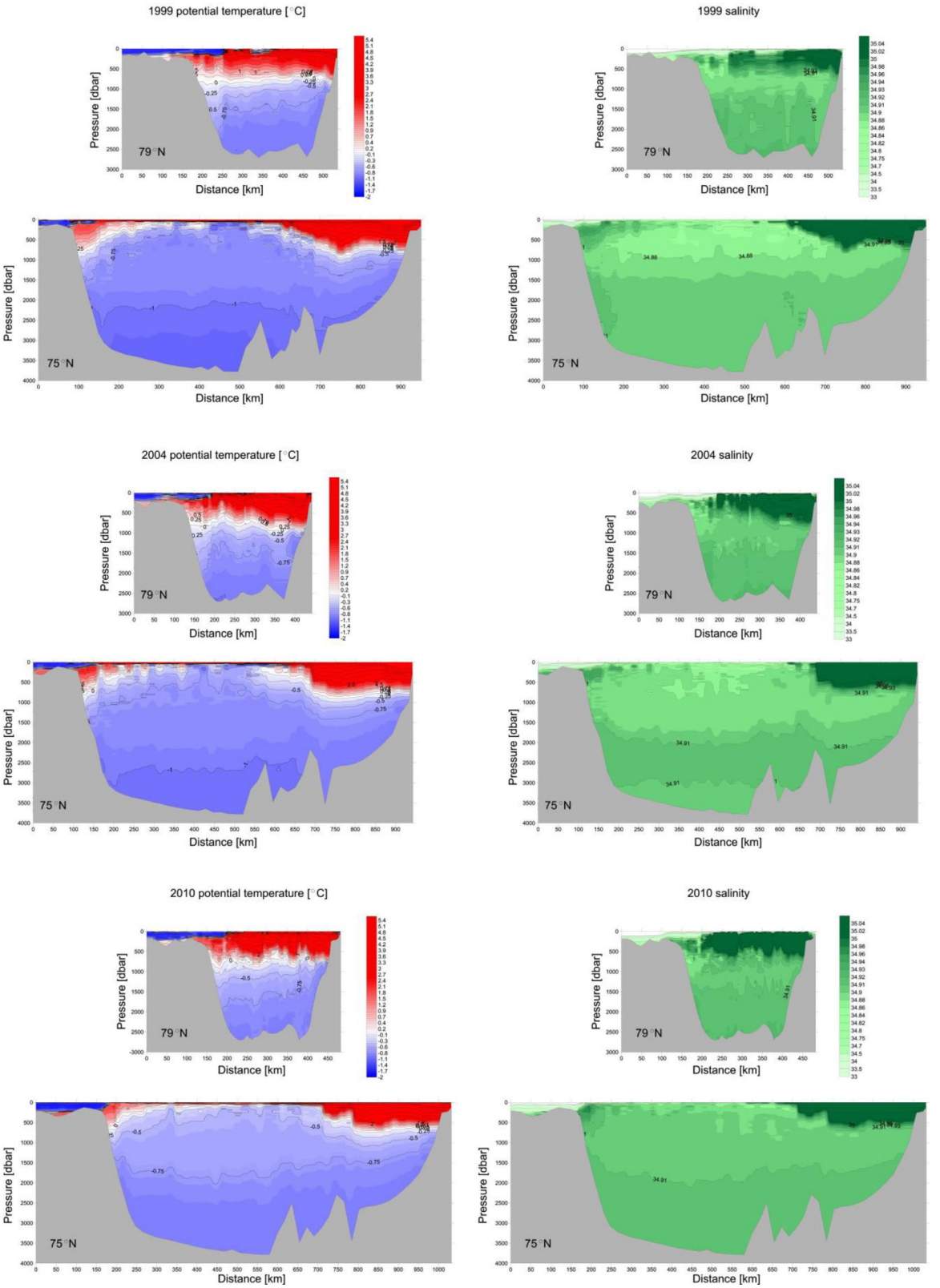

Figure 10. Sections of potential temperature, salinity, and velocity as end points, (b) Constant vertices at 1999 level, except AIW varies annually. with four constraints applied (1999, 2004, and 2010), and with the Argo adjustment and four constraints applied (1999–2010).

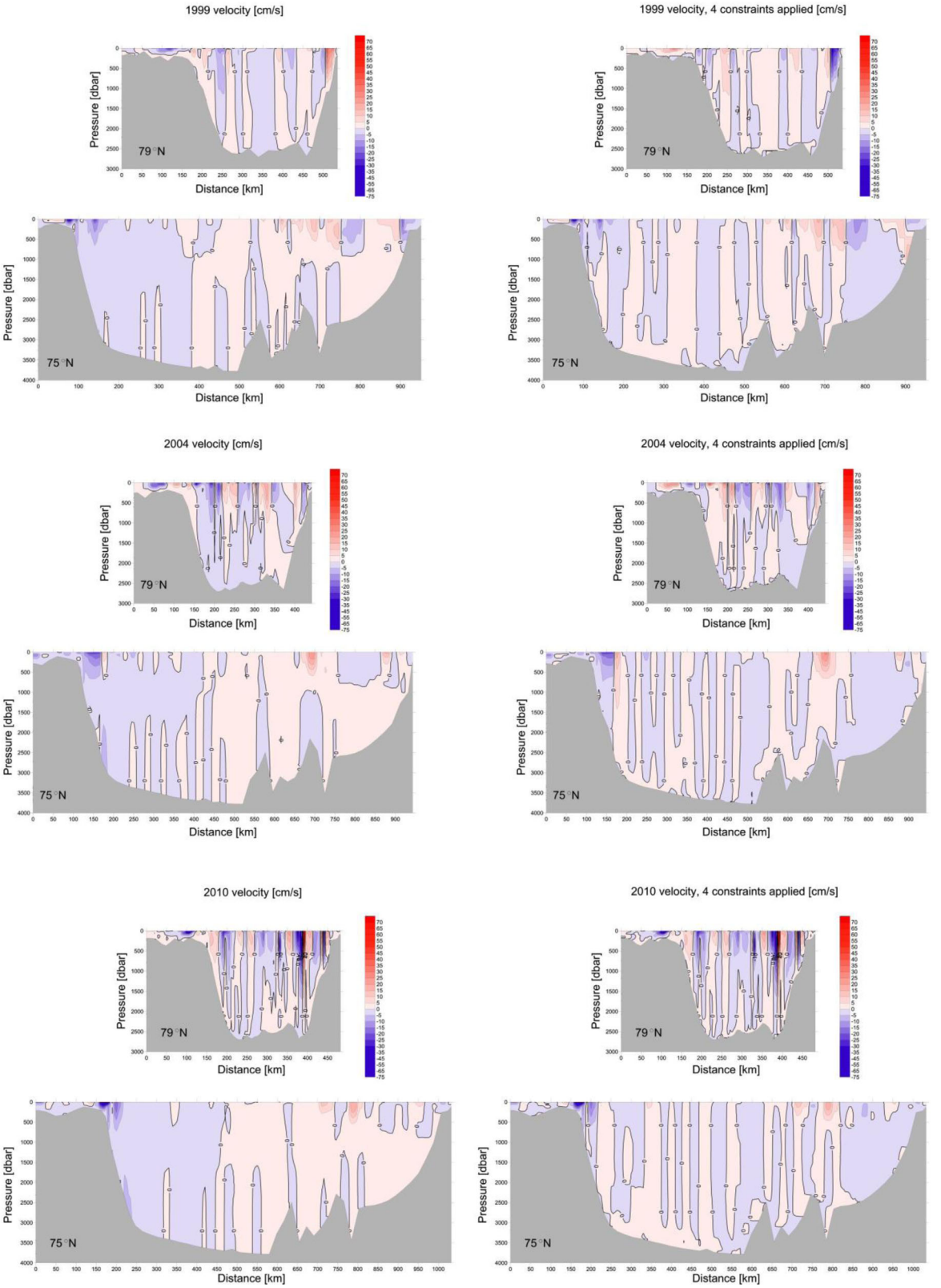

Figure 10. (continued)

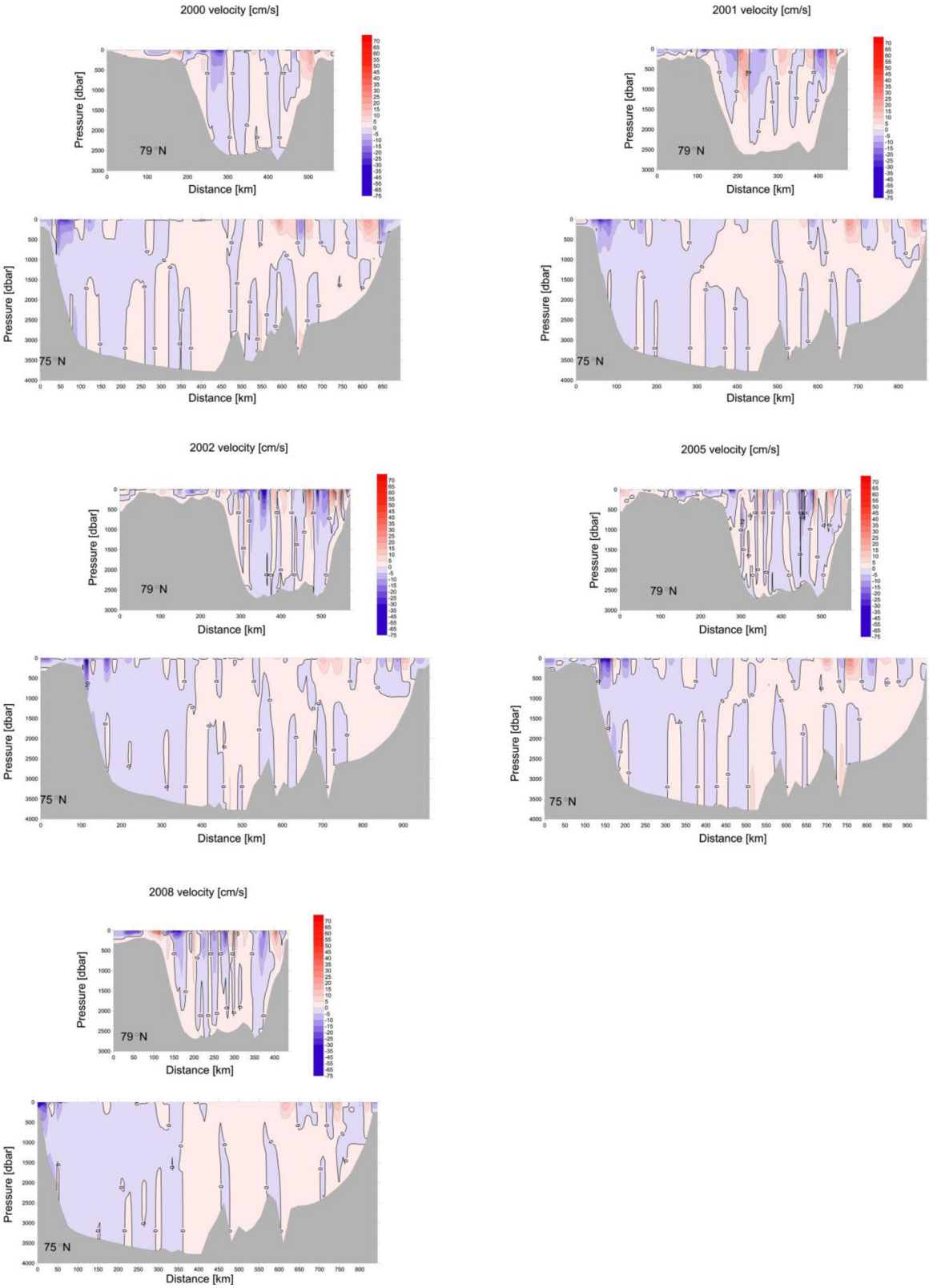

Figure 10. (continued)

in the near constant salinity layer above bottom (Figure 2a and Table A3). Vertical salinity and temperature gradients (gradS and gradθ) are computed between the salinity maximum and the deep layer as

$$\mathrm{grad}S = \left(S_{\mathrm{max}} - S_{\mathrm{deep}}\right)/h_{\mathrm{grad}} \text{ and} \tag{6}$$

$$\mathrm{grad}\theta = \left(\theta_{\mathrm{Smax}} - \theta_{\mathrm{deep}}\right)/h_{\mathrm{grad}} \tag{7}$$

where S_{max} (θ_{max}) is the salinity (potential temperature) at the deep salinity maximum, S_{deep} (θ_{deep}) is the salinity (potential temperature) of the homogeneous bottom layer, and h_{grad} is the thickness of the gradient layer below the salinity maximum (Figure 2a). If the bottom layer is homogeneous a turbulent vertical diffusion coefficient K_vS (K_vT) can be estimated from the temporal changes between the salinity (potential temperature) at the salinity maximum and the deep layer.

$$K_vS = \left(S_{\mathrm{deep}}(t_2) - S_{\mathrm{deep}}(t_1)\right) \cdot \frac{(h_{bl}(t_1) + h_{\mathrm{bl}}(t_2))/2}{(t_2 - t_1)(\mathrm{grad}S(t_1) + \mathrm{grad}S(t_2))/2} \tag{8}$$

$$K_v\theta = \left(\theta_{\mathrm{deep}}(t_2) - \theta_{\mathrm{deep}}(t_1)\right) \cdot \frac{(h_{bl}(t_1) + h_{bl}(t_2))/2}{(t_2 - t_1)(\mathrm{grad}\theta(t_1) + \mathrm{grad}\theta(t_2))/2} \tag{9}$$

where h_{bl} is the thickness of the bottom layer and t_1 is the time of the first observation and t_2 is the time of the second observation.

The amount of Arctic Ocean deep waters entering the central Greenland Sea from the rim is estimated from the differences between salinities at the salinity maximum in the rim and in the center of the Greenland Sea gyre using the diffusion coefficient K_vS following *Meincke et al*. [1997].

$$\frac{D\pi R^2 \Delta S_M}{t} = uD\frac{\pi R}{2}\Delta S_R - 2\pi R^2 K_V S\frac{\partial S}{\partial z} \tag{10}$$

where D is the thickness of the salinity maximum layer (averaged over the salinity maximum layers in the rim and in the central gyre over time), R is the Greenland Sea gyre radius, assumed to be 150 km, ΔS_M is the observed change over time of the salinity at the salinity maximum in the central Greenland Sea gyre, u is the zonal velocity component (positive from the rim towards the gyre center), and ΔS_R is the difference between the salinities averaged over the salinity maximum layer in the rim and in the central gyre. The transport from the rim toward the central gyre is assumed to take place over one quarter of the circumference of the gyre.

The Argo data reach a maximum depth of 2000 dbar which allows for the study of intermediate waters during all seasons. *Bönisch et al*. [1997] found only small variations in their intermediate waters (200–2000 m) between 1952 and 1980, and a warming trend from 1981 onward with only small variations in salinity. Since then Atlantic water properties and volumes have changed and the variations have become larger [*Karstensen et al*., 2005; *Latarius and Quadfasel*, 2010; *Walczowski et al*., 2012]. The seasonal (Figure 2b) and annual progress of convection in the Greenland Sea can be followed in the Argo data available for the Greenland Sea from 2001 onward for the convection has mainly been shallower than 2000 dbar during the recent years except for in some narrow coherent vortices [e.g., *Beszczynska-Möller and Dye*, 2013].

4. Results

4.1. Volume Transports

The net volume transports obtained from geostrophy and with four constraints applied for 8 years between 1999 and 2010, are -1.9 ± 1.0 Sv (southward) (Table 2, Figure 5). The individual northward and southward volume transports are larger through the GS section (14 ± 2 Sv northward and 16 ± 2 Sv southward) than through the FS section (9 ± 3 Sv northward and 11 ± 3 Sv northward) except in 2010 when both the northward and southward transports through the FS section are 3–4 Sv larger than during any of the other years. Net transports are southward in all years.

The net volume transports estimated using the linear fit to Argo float velocities and then applying four constraints average to -0.8 ± 1.5 Sv (southward) (Table 2). The northward and southward volume transports through the Fram Strait and southward volume transports through the Greenland Sea section average at

approximately the same as without adjusting the velocities with Argo data, and the northward transports through the Greenland Sea section 1–2 Sv larger. The net volume transports are southward, except in 2001 northward. *Fieg et al.* [2010] report a net southward volume flux from moorings in the Fram Strait in 1997–2005 to be 1.75 ± 5.01 Sv and from a fine resolution model 2.0 ± 1.26 Sv. The net volume flux from the same moored array but averaged over the period concurrent with the present study (1999–2010) is 2.8 ± 3.5 Sv southward (updated time series from *Schauer and Beszczynska-Möller* [2009]). Using a pan-Arctic inverse model for summer 2005, *Tsubouchi et al.* [2012] estimate the net volume transport through the Fram Strait at 1.6 ± 3.9 Sv southward. This result is lower, but considering the large variability, still in the same range.

The volume transports are estimated through five section parts. The net volume transports are 0.4–0.5 Sv southward in the Greenland shelf at both the FS and GS sections. The net volume transport is northward in the eastern slope at both the FS and GS sections, and also in the eastern half of the Greenland Sea deep basin, and southward elsewhere. The Argo adjustment enhances the northward volume transports in the eastern Greenland Sea and southward volume transports in the western Greenland Sea as would be expected across a line through a cyclonic gyre. The net volume transports at the Greenland Sea section parts become 5 Sv through each, southward at the two western section parts and northward at the two eastern section parts, with the largest variability in the east (Figure 7).

4.2. Heat and Freshwater Transports

Heat loss between the GS and FS sections is estimated at 9 ± 12 TW (Figure 8). Although the northward flowing surface water and AW at the Greenland Sea section are mainly warmer than at the Fram Strait section, most of them do not continue northward to the Fram Strait, but follow a cyclonic path at the rims of the Greenland Sea. This cyclonic path can be seen in the drift estimated from Argo floats during summer months (Figure 3). A larger cycle is captured by Argo float WMO# 6900303 (Figure 9). The northward flowing surface waters in the western slopes are about 0.5°C cooler at the FS section than at the GS section and AW is cooled about 0.1°C on its northward way between the sections.

Liquid freshwater transports are estimated relative to salinity 34.9. A net southward freshwater transport is found that is larger at the FS section, 66 ± 9 mSv, than at the GS section, 54 ± 20 mSv (Figure 8). The freshwater transport at the FS section compares well with the estimate by *de Steur et al.* [2009], who obtained an annual mean freshwater flux of 66 mSv (comprising 40.4 ± 14.4 mSv measured in the East Greenland Current by a moored array and 25.6 ± 11.3 mSv estimated for the East Greenland shelf). The salinities of the southward flowing surface waters, where most of the freshwater transport lies, are higher in the GS than in the FS section. On average 12 mSv of freshwater is lost between the two sections.

4.3. Water Mass Transports, Properties, and Transformations

Volume transports are estimated for six water mass classes [*Rudels et al.*, 2005, 2008]. Net volume transports give a reasonable southward flow of 1–2 Sv (Table 2) as compared with previous estimates, but some of the individual water mass transports seem questionable, e.g., a larger net volume transport of AW northward through the FS than through the GS section during some of the years (Figure 6). The transports with the Argo adjustment and four constraints applied are presented in the text below from surface to bottom.

The surface water net volume transports are southward through both the FS and GS sections with an average of 0.6–0.7 Sv. The net transports through the GS section are larger than those through the FS section in 2002 and 2010, which could be explained by melting between the sections, an interpretation supported by a net freshwater input between the sections in 2002 (Figure 8). In 2008, the net volume transport of surface water is larger through the FS section, which could be due to the missing East Greenland shelf at the GS section where a substantial amount of surface water is estimated to flow southward during most of the other years (Figure 10, velocities). During the other years, the net volume transports of surface water through the two sections are within ±0.1 Sv of one another (Figures 6 and 7). Separating the sections to a western and eastern part at 0 meridian gives a net southward volume transport of surface water in the western FS section 0.86 Sv and GS section 1.21 Sv, and in the east a net northward transport in FS section 0.19 Sv and in GS section 0.36 Sv.

Net AW volume transports are estimated at about 0.9 Sv northward through the GS section and 0.7 Sv northward through the FS section (Figure 6). Over the observation period from 1999 to 2010 AW has become about 0.4°C warmer and over 0.005 more saline (Figure 7). At the GS section, the temperature

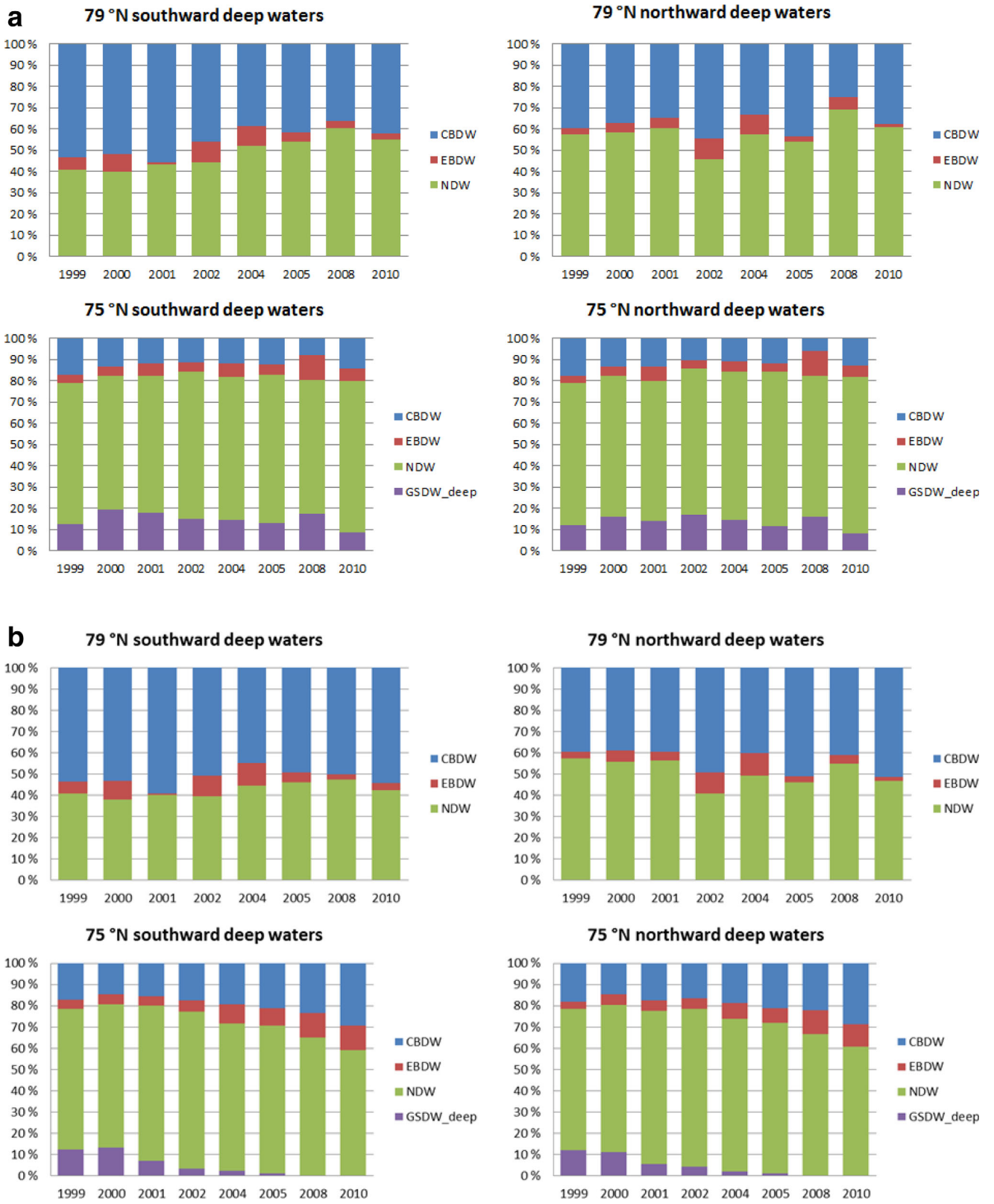

Figure 11. Deep water volume transport proportions by water mass using the triangle division with (a) annually varying triangle vertices (water mass end-members), (b) constant triangle vertices at 1999 level, except AIW varying annually.

difference between northward and southward flowing AW is above 0.5°C and in FS the difference has diminished from about 0.4 to 0.1°C. The difference in the Fram Strait getting smaller could be interpreted as AW making a shorter loop north of the FS section at the end of the observation period, or cooling less. A likely cause for the decreasing temperature difference in the Fram Strait is the significantly warmer westward recirculation of Atlantic water directly in the Fram Strait in the late 2000s as reported by *Beszczynska-Möller et al*. [2012] and *de Steur et al*. [2014]. Another cause could be the presence of more or stronger eddies since in 2010 the AW northward and southward transports at the FS section are both about 7 Sv as compared with the 2–5 Sv during the other years (Figures 6 and 10, velocities). AW at the GS section is warmer and more saline than at the northern FS section. The warmest and most saline AW is found to flow northward through GS section and the coolest and least saline southward through FS section. The southward flowing AW is not systematically warmer and saltier at either section, the properties depending on how much cooling and mixing the water mass has undergone. A seasonal cycle has been observed in AW by e.g., *Latarius and Quadfasel* [2010] and by *Beszczynska-Möller et al*. [2012]. The FS section is taken immediately, or within a month or two, after the GS section but both observations are still made in summer and the differences due to seasonality between the two sections is expected to be small.

Separating the sections into 4–5 parts allows for following the water masses in more detail (Figure 7). The warmest and most saline AW (e.g., in 2010 3.93°C, 35.11) is found flowing northward in the eastern slope of the GS section, while a large part with similar properties flows southward west of it, suggesting a large-scale eddy structure. The northward flowing AW in WSC in FS is already slightly cooler and less saline (in 2010 3.63°C, 35.09). The AW flowing southward in the western FS is significantly cooler and less saline (in 2010 1.81°C, 34.90), and the southward flowing AW in the western GS section is again slightly cooler and less saline (in 2010 1.65°C, 34.90).

The net volume transports of dAW are estimated at 0.5 Sv southward through the whole FS section and 0.8 Sv southward through the GS section. Over the study period, dAW has become warmer and more saline (Figure 7). The dAW in the FS section is warmer and more saline than in the GS section. This could be due to AW being cooled between the two sections, becoming denser, and entering the dAW range. Northward flowing dAW is more saline and warmer than southward flowing.

The effect on intermediate water transports of the choice between using Argo adjustment or not is 3.0 Sv in the GS section. The level at which the Argo adjustment is applied to the velocities, 1000 dbar, is mostly located within the intermediate water layer of *Rudels et al*. [2008]. The individual northward and southward volume transports at the GS section decrease to about 3 Sv after the Argo adjustment, remaining 1.4 Sv larger than at the FS section. The net volume transport of intermediate water however is about 0.5 Sv southward with both methods (Figure 6). The intermediate water contains both AIW originating from the Nordic Seas and upper Polar Deep Water (uPDW) originating from the Arctic Ocean, a separation between the two has not been attempted. The intermediate waters have become warmer and more saline over the observation period at the GS section but show no clear trend at the FS section. Intermediate waters are warmer and more saline at the FS section than at the GS section, and the difference gets smaller between 1999 and 2010, starting from above 0.2°C for temperature and 0.02–0.03 for salinity and ending at about 0.1°C and very small or no difference in salinity (Figure 7).

The deep waters can be separated into two classes based on their densities (Table A2). The net deep water volume transports are close to zero, being sometimes southward and sometimes northward. The density division alone does not allow for distinguishing between the Arctic Ocean and the Nordic Seas deep water masses. The deep waters are observed, both in the Greenland Sea [*Somavilla et al*., 2013] and in the Fram Strait [*Langehaug and Falck*, 2012] to be warming and becoming more saline. Using the definitions by *Rudels et al*. [2008] and separating between EBDW, CBDW, and NDW at salinity 34.915 seems to work best, as estimated visually, in mid-2000s (Figure 4). Since 2007 parts of the NDW have become more saline than the 34.915 limit of *Rudels et al*. [2008] and *Marnela et al*. [2013] and in 2013 the salinity of GSDW, part of NDW, is already close to 34.92, a limit used for separating between Arctic Ocean and Nordic Seas originated waters by e.g., *Langehaug and Falck* [2012]. The EBDW can have salinities up to 34.93 in FS and it is no longer possible to distinguish between the Arctic Ocean and Nordic Seas originated deep water masses merely based on their salinities and temperatures without at least inspecting the individual θS curves. *Von Appen et al*. [2015] have noted that the different deep waters present in Fram Strait have become more similar and estimated for the deep waters of the northern and southern origins to have the same temperature in Fram Strait in 2020. The salinities are getting similar too (Figure 4).

The deep water masses are more saline and warmer at the FS section than at the GS section (Figure 7). The deep waters have in general become warmer and more saline, with the largest changes observed in the Greenland Sea, about 0.01°C/yr in temperature and 0.007/yr in salinity. The less dense deep water flowing southward through the FS section however has become colder and less saline. This could be due to CBDW, the warmest of the deep waters becoming more diluted with colder and less saline AIW or NDW.

Deep waters are distinguished using the triangle method [*Mamayev*, 1975] with potential temperature and salinity values dedicated to a specific water mass at the vertices of the triangles. These end points are allowed to vary annually (see Figure 4 for how the annually varying triangle vertices are defined). The water mass triangles also affect the intermediate water transports by up to 1 Sv due to the changing lower limit of the defined intermediate water layer. Allowing the triangle end points to vary annually shows a decrease in the Fram Strait CBDW volume transport proportion of deep waters flowing southward from 50% to about 30–40% (Figure 11a). The decrease could at least partially be caused by the big changes in AIW properties with AIW becoming warmer and more saline and thus more similar to CBDW whose properties remain nearly constant (and in this work are kept constant). EBDW volumes are very small and the southward volume transport also decreases during 1999–2010. The southward flowing volume proportion of NDW increases as the fraction of Arctic Ocean waters diminishes. NDW, including the small amounts of deep GSDW, represents about 60–70% of the northward flowing deep waters in the Fram Strait. No clear trends are found in the northward flow in the FS section. In the GS section no clear increase or decrease of transports of any specific deep water mass is found and the NDW constitutes 80% of the deep waters.

The volume transports for the deep waters are also estimated fixing the triangle vertices to values from 1999, except for AIW which is allowed to vary annually, to estimate the changes in the proportional water mass volumes that have taken place in over a decade. NDW in the Greenland Sea has become warmer and more saline, from the late 1970s to 2013 the salinity has increased from 34.89 to 34.918 and potential temperature from -1.28°C to -0.95°C. Over the observation period 1999–2010, salinity increased from 34.902 to 34.914 and temperature from -1.16°C to -1.00°C (Table 1 and Figure 4). In the Greenland Sea, the NDW volume transport, including the deep GSDW, therefore decreases from 80% to 60% while the Arctic Ocean deep waters increase from 20% to 40% (Figure 11b). In the Fram Strait, the changes are small.

4.4. Mixing

Mixing in the Greenland Sea is estimated in the same way as in *Meincke et al*. [1997] between the deep salinity maximum and the near bottom homogeneous layer. The mean vertical salinity gradient between the two years 1982 and 1993 given in *Meincke et al*. [1997] is $4.4{\cdot}10^{-6}$ m^{-1} and computed from their values $5.1{\cdot}10^{-6}$ m^{-1}. From salinities between 1999 and 2010, a salinity gradient of $4.0{\cdot}10^{-6}$ m^{-1} is estimated and from temperatures a temperature gradient of $9.5{\cdot}10^{-5}$°C·m^{-1}.

Using data in Table A3 for the observation period from 1999 to 2010 K_vS(99-10) is estimated at $1.6{\cdot}10^{-3}$ m^{2}s^{-1} and K_vT(99-10) at $8.5{\cdot}10^{-4}$ m^{2}s^{-1}. The values are smaller than those of *Meincke et al*. [1997] who obtained $3.7{\cdot}10^{-3}$ m^{2}s^{-1} for K_vS, but the ratio of K_vS:$K_vT = 2$:1, is the same.

Meincke et al. [1997] estimated a 0.3 Sv inflow of EBDW to the Greenland Sea from their K_vS of $3.7{\cdot}10^{-3}$. In this work for the whole available period from 1977 to 2013, an averaged value of $2.3{\cdot}10^{-3}$ m^{2}s^{-1} is estimated for the vertical diffusivity from salinities, and for 1999–2010 $1.8{\cdot}10^{-3}$ m^{2}s^{-1}. The value is larger in the beginning, $6.2{\cdot}10^{-3}$ m^{2}s^{-1} averaged for 1977–1988 (Table A3). The velocity from the rim of the Greenland Sea to the center is estimated in a way following *Meincke et al*. [1997] at 0.8 ± 0.5 cm/s for a period of 1999–2006. From 2008 onward, the salinity differences at the salinity maximum layers at the rim and in the central Greenland Sea are too small, or the salinity is smaller in the rim, to make this kind of estimation. The volume transport of EBDW into the central Greenland Sea gyre is estimated averaged over 1999–2006 at about 0.9 ± 0.6 Sv. More than the 0.44 ± 0.09 Sv estimated by *Somavilla et al*. [2013], but in the same range as estimated by Jeansson et al. (personal communication, 2016) based on salinity differences between 1982 and 2002.

5. Summary and Discussion

The amount of Arctic Ocean waters transported to the Nordic Seas as well as the amount of waters transported through Fram Strait to the Arctic Ocean, i.e., AW, intermediate waters formed in the Greenland Sea, and NDW, are estimated from geostrophy adjusted with Argo float velocities from summer, and by applying

four conservation constraints, and averaged over eight summers between 1999 and 2010. The adjustment uses a simple linear fit to the data although the transports in the center of the GS gyre are variable and at the rims the velocities observed by Argo floats are one order of magnitude larger than those estimated from the linear fit. The data are sparse and making another kind of fit would have required guesses and those guesses would then affect the resulting transports. The effects of the slope of the linear fit were studied (not shown) and it was found that changing the slope steepness originally of 0.0012 by 0.0002 ((m/s)/longitude), alters the net volume transport by about 0.2 Sv, with the net transport diminishing as the slope increases, and the northward and southward transports at the GS section increasing correspondingly by on average 0.8 Sv (southward flow) and 1.0 Sv (northward flow). At the FS section for every 0.0002 change in the slope steepness, the northward flow increases by about 0.1–0.2 Sv and the southward flow decreases slightly. The results obtained for the volume transports are thus rather sensitive to how the adjustment based on Argo data is conducted. The net volume transports estimated in this study, 0.8 ± 1.5 Sv southward, are from a low range as compared with the recent estimates of 2–3 Sv southward for the Fram Strait. Future studies with better Argo coverage could improve the estimates based on similar methods as presented in this work. The drift estimated from the Argo floats is also available as an ANDRO product at http://wwz.ifremer.fr/lpo/Produits/ANDRO. The linear fit was estimated from the ANDRO data for comparison and increased the slope from 0.0012 to 0.0014.

The water mass definitions used here follow those by *Rudels et al*. [2005, 2008] for surface water and Atlantic waters. However, their deep water definitions separating the Arctic Ocean originated and Nordic Seas originated waters at salinity 34.915 are no longer valid for the most recent years due to the warming and salinification of GSDW, reported by for example, *Somavilla et al*. [2013]. A water mass triangle approach is therefore used for distinguishing between deep waters of different origin. The sections are separated into 4–5 parts to better distinguish the differences in the northward and southward flows.

The surface water net volume transport is 0.7 Sv southward. The least saline waters, partly due to ice melt, are found in the surface layer. Most of the liquid freshwater transport is therefore located in the surface layer. Liquid freshwater is accumulated in the area between the FS and GS sections, i.e., the southward freshwater transports at the FS section are larger than the southward freshwater transports at the GS section contrary to what might be expected should ice melt in the area between the sections. The observations are from summer time and no sea ice formation therefore expected to remove liquid freshwater from the area. However, there is a net heat loss between the sections and ice formation cannot be completely ruled out. The individual northward and southward freshwater transports at the GS section relative to salinity 34.9 are smaller than corresponding transports at the FS section so the freshwater does not appear to be caught in a cyclonic flow at the GS section either. An explanation might be the later observation time of the FS section which would allow for more ice melt to have taken place at the FS section. The surface water properties, colder, and less saline at the FS than at the GS section (Figure 7), also support this hypothesis. Advection of these melt waters southward to the GS section also introduces an additional time lag.

The time lag for waters traveling from one section to the other has been ignored. The Argo floats located in the Nordic Seas show travel times at 1000 dbar level of about 2–3 months from the Fram Strait to 75°N in the EGC and from 2 months to a year in the opposite direction. The effect of the near surface drift on the estimated Argo float drift at the intermediate depths was estimated by *Voet et al*. [2010] as max 5 km during the 10 day cycle that the float makes. This and the other inaccuracies related to the use of Argo float data are described in *Voet et al*. [2010] and here ignored, yet causing a small error.

The AW volume transports are estimated at about 0.9 Sv northward through the GS section and 0.7 Sv northward through the FS section and dAW transports at 0.5 Sv southward through the FS section and 0.8 Sv southward through the GS section. Both the AW and dAW have become warmer and more saline during 1999-2010. Previous studies by e.g., *Beszczynska-Möller et al*. [2012] show a maximum in the AW temperature and salinity in 2006 and a 5–6 year cycle in the AW properties, and warm and saline AW has been observed e.g., in 1984, perhaps taking away some of the significance of the trend observed in 1999–2010. When the sections are separated into 4–5 parts, the northward AW flow can be seen in the eastern sides of the sections while somewhat cooled and diluted AW is found to return southward in the western sides (Figure 7). A substantial amount of the heat transport takes place within the AW. Heat is estimated to be lost between the two sections by about 9 ± 12 TW. Somewhat less than the 12.7 TW estimated by *Cisewski et al*. [2003] from 1997 data to be lost between a 75°N section and a section in the Fram Strait at 79°40′N, and

Table A1a. Cruises the Hydrographic Data for the Zonal Double Sections at the Greenland Sea (GS) and the Fram Strait (FS) Are Obtained From

Ship, Cruise	Year and Month of the FS Stations	Number of Stations at the FS Section	Longitudes °W/°E Covered by the FS Section	Latitudes °N Covered by the FS Section
Polarstern, ar15	1999 Sep	38	−13.24 to 9.01	78.83–79.17
Lance	2000 Aug–Sep	35	−15.00 to 10.99	78.92–79.02
Polarstern, ar17	2001 Jul	39	−11.77 to −10.01	78.83–79.02
Polarstern, ar18	2002 Jul–Aug	73	−17.48 to 9.00	78.82–78.84
Polarstern, ar20	2004 Jul–Aug	49	−11.47 to 9.00	78.83–78.84
Polarstern, ar21	2005 Aug–Sep	76	−17.48 to 9.01	78.81–78.84
Polarstern, ar23	2008 Jul	58	−10.99 to 9.01	78.82–78.85
Polarstern, ar25	2010 Jul	79	−12.51 to 9.83	78.83–78.84
Ship, Cruise	**Year and Month of the GS Stations**	**Number of Stations Available at the GS Section**	**Longitudes °W/°E Covered by the GS Section**	**Latitudes °N Covered by the GS Section**
Polarstern, ar15	1999 Jul	60	−15.93 to 17.10	74.99–75.01
Polarstern, ar16	2000 Jul	57	−13.68 to 17.10	74.92–74.98
Polarstern, ar17	2001 Jun–Jul	52	−14.36 to 15.89	74.96 to 75.01
Polarstern, ar18	2002 Jul	62	−16.42 to 17.10	75.00
Polarstern, ar20	2004 Jun–Jul	55	−16.74 to 15.84	75.00–75.08
Polarstern, ar21	2005 Jul–Aug	56	−17.09 to 15.82	74.99–75.01
Polarstern, ar23	2008 Jun	52	−12.61 to 16.50	75.00–75.19
Polarstern, ar25	2010 Jun	62	−17.99 to 17.00	74.60–75.01

similar in magnitude to the about 11 TW estimated to be lost from a smaller area north of the FS section by Marnela et al. [2013]. Some of the heat carried by AW continues northward past the Fram Strait while some remains or is lost in the Nordic Seas. In this study, the budget for the Arctic Ocean is not closed and the heat transports computed relative to a reference temperature through the individual sections are arbitrary [see *Schauer and Beszczynska-Möller*, 2009; *Tsubouchi et al*., 2012]. The FS and GS sections are treated as synoptic, but in fact they are not since the southern section is taken first and some of the northward transport may even be observed twice, first at the GS and later at the FS section. Sometimes the waters can get caught in an eddy as revealed by the Argo floats and take much longer, up to a year, between the sections. Only a few Argo floats were carried into the Fram Strait from the Greenland Sea. They did not coincide with the times of the hydrographic observations, and a more detailed study would be required to include them into the present analysis.

The intermediate water transports are in this study affected by the choices of whether to use Argo adjustment or not, and also by the deep water mass definitions. The net volume transport of intermediate water is estimated at about 0.5 Sv southward. The intermediate waters have become warmer and more saline at the GS section, thus decreasing the difference between the intermediate waters found in the two sections. The intermediate waters have not here been separated into AIW and uPDW, although AIW as observed in the Greenland Sea is used as a vertex for the water mass triangles. The separation between AIW and uPDW could be possible to some extent based on their (θS) curves, or using additional parameters that have not been included in this study.

A temperature maximum in the intermediate waters in the Greenland Sea which appeared in the beginning of the 1990s at the depth of 800 m had its origins in the Amerasian Basin warm waters. The intermediate temperature maximum gradually descended downward [e.g., *Meincke et al*., 1997; *Budéus et al*., 1998; *Somavilla et al*., 2013] (Figure 4). In 2005, another maximum appeared above it. Temperature maxima can be created during shallow convection and descend downward unless erased by deeper convection events or lateral advection in the following years. The 1990s pulse has already reached deep and its temperature maximum has disappeared because of the temperature increase in the layers above.

Convection depths were estimated from CTD profiles and Argo data. Data from Argo floats allow for tracking the seasonal development of the convection. Since the Argo floats have been collecting data from the Nordic Seas, some coherent vortices reaching deeper than the Argo floats profiles (i.e., below 2000 dbar), have been present, e.g., in 2002 extending down to 2500 dbar. These depths cannot be covered with the regular Argo floats, but deep profiling Argo floats would be needed. Mainly the convection has been

Table A1b. Other Cruises/Sources for Hydrographic Data From the Greenland Sea (GS), the Norwegian Sea (NS), and the Fram Strait (FS)

Ship, Cruise or Source	Year, Month	Area
Pangaea.de	1977, 1978	GS
WOD13_CA	1982 Mar	FS, GS, NS
Pangaea.de	1984, 1988	GS
WOD13_NO/Polarstern, ar09	1993 Nov/Mar	NS, GS/FS
Pangaea.de	1994–1998	GS
WOD13_NO	1999 Jun	NS
WOD13_NO	2000 May	NS
WOD13_NO	2001 Jun	NS
WOD13_NO	2002 Jun	NS
Polarstern, ar19	2003 Apr–May	GS
WOD13_NO	2005 Apr	NS
WOD13_NO/Maria S Merian, ar22	2006 May/Jul–Aug	NS/FS, GS
IPY database	2008 Jul	NS
Polarstern, ar24	2009 Jun–Jul	FS, GS
WOD13_NO	2011 Jun, Sep	GS east, NS, FS east
Oceania, IOPAN AREX'12	2012 Jun, Jul	GS east
WOD13_NO/Oceania, IOPAN Arex'13	2013 May, Jul/Jul	NS, GS/FS east

shallower than 2000 dbar and the seasonal evolution can be observed in the Argo data starting in the autumn with cooling waters gradually mixing deeper. Surface waters reach temperatures near freezing point in November and December [*Visbeck et al*., 1995], and the maximum convection depth is reached in the spring (Figure 2). Should the convection reach deeper than the Argo floats maximum profiling depth, some small changes in the potential temperature and salinity properties might be detectable. The effect of having chosen 1900 dbar as the Greenland Sea maximum convection depth during 1999–2010 and used as a limit for the constraints was tested (not shown). The effect of changing the limit by 100 dbar is small, reducing the net volume transports by 0–0.1 Sv. Changing the limit by 300 dbar results in a reduction of 0.1–0.3 Sv.

Over the past two decades, the deep waters in the Fram Strait have warmed substantially more (about 0.1°C) than the source waters in the Arctic Ocean (0.02°C). The Norwegian Sea deep water has become slightly less than 0.1°C warmer while the Greenland Sea deep water has warmed by 0.2°C. The deep waters in the Fram Strait, unlike in the central Greenland or Norwegian Seas (Lofoten Basin) show properties over a wide range and *von Appen et al* [2015] observe substantial mixing of deep waters in the Fram Strait itself. The Fram Strait stations for Figure 4 were chosen rather arbitrarily with an attempt to keep their number down to two and to include maximal and minimal salinity values, often excluding waters with e.g., clear Norwegian Sea Deep Water properties (yellow lines in Figure 4). The two stations should therefore not be considered representative for the eastern or western parts of the strait. The bottom density development toward less dense waters can yet be observed in Figure 4.

The deep water mass transports are estimated using water mass triangles. The results are affected by how the vertices are chosen. We have chosen them as close to the waters observed as possible but yet altering

Table A2. Water Mass Definitions of *Rudels et al*. [2008]

Water masses	Density Range	Nordic Seas Water Masses	Arctic Ocean Water Masses
Surface water	$\sigma_\theta < 27.70$	Warm Surface Water (wSW)	Polar Surface Water (PSW)
Atlantic water	$27.70 \leq \sigma_\theta < 27.97$	Atlantic Water (AW)	Arctic Atlantic Water (AAW)
Dense Atlantic water	$\sigma_\theta \geq 27.97$	dense Atlantic Water (dAW)	dense Arctic Atlantic Water (dAAW)
	$\sigma_{0.5} < 30.444$, $\theta > 0$	S and θ decreasing with depth	S increasing, θ decreasing with depth
Intermediate water	$\sigma_\theta \geq 27.97$, $\sigma_{0.5} < 30.444$, $\theta \leq 0$	Arctic Intermediate Water (AIW)upper S and θ decreasing with depth, lower S and θ increasing with depth	upper Polar Deep Water (uPDW) S increasing, θ decreasing with depth.
Deep Water I	$\sigma_{0.5} \geq 30.444$, $\sigma_{1.5} < 35.142$	Nordic Seas Deep Water I (NDWI), S<34.915	Canadian Basin Deep Water (CBDW)
Deep Water II	$\sigma_{1.5} \geq 35.142$	Nordic Seas Deep Water II (NDWII), S<34.915	Eurasian Basin Deep Water (EBDW)

Table A3. Greenland Sea Deep Salinity Maximum Properties and the Depth of Its Location, the Salinity of the Bottom Layer Below the Gradient and the Thickness of the Layer, and the Thickness of the Gradient Layer in Between[a]

a)

Year	$-z\ S_{max}$	S at S_{max}	S deep	h gradient	h bottom layer	Vertical S gradient	K_vS	D of S_{max}	S at S_{max} rim	D of S_{max} rim	u (cm/s)	Vol
1977	1500	34.894	34.890	1000	1200	$4.0{\cdot}10^{-6}$						
1978	1300	34.896	34.892	1400	1000	$2.9{\cdot}10^{-6}$	$2.0{\cdot}10^{-2}$					
1982	1500	34.896	34.892	1000	1200	$4.0{\cdot}10^{-6}$	0					
1984	2200	34.900	34.894	1300	200	$4.6{\cdot}10^{-6}$	$5.2{\cdot}10^{-3}$					
1988	2400	34.897	34.893	800	500	$5.0{\cdot}10^{-6}$	$-5.8{\cdot}10^{-4}$					
1993	2400	34.905	34.900	800	400	$6.3{\cdot}10^{-6}$	$3.5{\cdot}10^{-3}$	490	34.912	400		
1994	2500	34.903	34.899	1000	200	$4.0{\cdot}10^{-6}$	$-1.8{\cdot}10^{-3}$	620	34.909	440		
1995	2400	34.905	34.900	1100	200	$4.5{\cdot}10^{-6}$	$1.5{\cdot}10^{-3}$	660	34.910	660	0.59	0.83
1996	2400	34.906	34.901	1100	200	$4.5{\cdot}10^{-6}$	$1.4{\cdot}10^{-3}$					
1997	2000	34.904	34.898	1400	300	$4.3{\cdot}10^{-6}$	$-5.4{\cdot}10^{-3}$					
1998	2000	34.906	34.900	1300	300	$4.6{\cdot}10^{-6}$	$4.3{\cdot}10^{-3}$	560	34.908	400	0.51	0.69
1999	2200	34.907	34.902	1200	300	$4.2{\cdot}10^{-6}$	$4.3{\cdot}10^{-3}$	570	34.911	600	1.31	1.64
2000	2250	34.908	34.9025	1300	150	$4.2{\cdot}10^{-6}$	$8.5{\cdot}10^{-4}$	400	34.911	430	0.44	0.52
2001	2250	34.909	34.903	1250	200	$4.8{\cdot}10^{-6}$	$6.1{\cdot}10^{-4}$	460	34.911	490	0.34	0.35
2002	2300	34.910	34.905	1250	150	$5.0{\cdot}10^{-6}$	$2.5{\cdot}10^{-3}$	400	34.912	590	1.07	1.23
2004	2500	34.9115	34.907	1000	200	$4.5{\cdot}10^{-6}$	$1.3{\cdot}10^{-3}$	510	34.914	500	0.53	0.61
2005	2600	34.912	34.908	950	150	$4.4{\cdot}10^{-6}$	$1.3{\cdot}10^{-3}$	410	34.915	650	0.49	0.60
2006	2500	34.9135	34.9095	1100	100	$3.6{\cdot}10^{-6}$	$1.5{\cdot}10^{-3}$	470	34.915	420	1.44	1.66
2008	2750	34.915	34.9125	650	250	$3.8{\cdot}10^{-6}$	$2.2{\cdot}10^{-3}$	380	34.915	480		
2009	2850	34.9155	34.9135	650	200	$3.1{\cdot}10^{-6}$	$2.1{\cdot}10^{-3}$	288	34.9155	539		
2010	2850	34.916	34.914	650	200	$3.1{\cdot}10^{-6}$	$1.0{\cdot}10^{-3}$	490	34.916	490		
2013	3100	34.919	34.918	400	200	$3.8{\cdot}10^{-6}$	$2.4{\cdot}10^{-3}$	400	34.919	300		
Mean						$4.2{\cdot}10^{-6}$	$2.3{\cdot}10^{-3}$					
Std						$7.6{\cdot}10^{-7}$	$4.6{\cdot}10^{-3}$					
Mean77–88						$4.1{\cdot}10^{-6}$	$6.2{\cdot}10^{-3}$					
Mean 93–99						$4.6{\cdot}10^{-6}$	$1.1{\cdot}10^{-3}$					
Mean 00–13						$4.0{\cdot}10^{-6}$	$1.6{\cdot}10^{-3}$					
Mean 99–10						$4.1{\cdot}10^{-6}$	$1.8{\cdot}10^{-3}$					

b)

Year	$-z\ S_{max}$	θ at S_{max}	θ deep	h gradient	h bottom layer	Vertical θ gradient	K_vT
1977	1500	−1.21	−1.27	1000	1200	$6.0{\cdot}10^{-5}$	
1978	1300	−1.16	−1.28	1400	1000	$8.6{\cdot}10^{-5}$	$-4.8{\cdot}10^{-3}$
1982	1500	−1.18	−1.29	1000	1200	$1.1{\cdot}10^{-4}$	$-8.9{\cdot}10^{-4}$
1984	2200	−1.18	−1.25	1300	200	$5.4{\cdot}10^{-5}$	$5.4{\cdot}10^{-3}$
1988	2400	−1.18	−1.24	800	500	$7.5{\cdot}10^{-5}$	$4.3{\cdot}10^{-4}$
1993	2400	−1.13	−1.21	800	400	$1.0{\cdot}10^{-4}$	$1.6{\cdot}10^{-3}$
1994	2500	−1.12	−1.20	1000	200	$8.0{\cdot}10^{-5}$	$1.1{\cdot}10^{-3}$
1995	2400	−1.09	−1.19	1100	200	$9.1{\cdot}10^{-5}$	$7.4{\cdot}10^{-4}$
1996	2400	−1.07	−1.17	1100	200	$9.1{\cdot}10^{-5}$	$1.4{\cdot}10^{-3}$
1997	2000	−1.00	−1.17	1400	300	$1.2{\cdot}10^{-4}$	0
1998	2000	−1.00	−1.17	1300	300	$1.3{\cdot}10^{-4}$	0
1999	2200	−1.01	−1.16	1200	300	$1.3{\cdot}10^{-4}$	$7.3{\cdot}10^{-4}$
2000	2250	−0.99	−1.14	1300	150	$1.2{\cdot}10^{-4}$	$1.2{\cdot}10^{-3}$
2001	2250	−0.98	−1.13	1250	200	$1.2{\cdot}10^{-4}$	$4.7{\cdot}10^{-4}$
2002	2300	−0.97	−1.11	1250	150	$1.0{\cdot}10^{-4}$	$1.0{\cdot}10^{-3}$
2004	2500	−0.98	−1.09	1000	200	$1.1{\cdot}10^{-4}$	$5.0{\cdot}10^{-4}$
2005	2600	−0.98	−1.07	950	150	$9.5{\cdot}10^{-5}$	$1.1{\cdot}10^{-3}$
2006	2500	−0.97	−1.06	1100	100	$8.2{\cdot}10^{-5}$	$4.4{\cdot}10^{-4}$
2008	2750	−0.96	−1.02	650	250	$9.2{\cdot}10^{-5}$	$1.3{\cdot}10^{-3}$
2009	2850	−0.96	−1.01	650	200	$7.7{\cdot}10^{-5}$	$8.4{\cdot}10^{-4}$
2010	2850	−0.95	−1.00	650	200	$7.7{\cdot}10^{-5}$	$8.2{\cdot}10^{-4}$
2013	3100	−0.93	−0.955	400	200	$6.3{\cdot}10^{-5}$	$6.0{\cdot}10^{-4}$
Mean						$9.5{\cdot}10^{-5}$	$6.7{\cdot}10^{-4}$
Std						$2.1{\cdot}10^{-5}$	$1.7{\cdot}10^{-3}$
Mean77–88						$8.1{\cdot}10^{-5}$	$3.5{\cdot}10^{-5}$
Mean 93–99						$1.1{\cdot}10^{-4}$	$8.0{\cdot}10^{-4}$
Mean 00–13						$9.4{\cdot}10^{-5}$	$8.3{\cdot}10^{-4}$

c)

Year	σ_0 at S_{max}	σ_0 bottom	σ_2 at S_{max}	σ_2 bottom
1977	28.078	28.082	37.466	37.484
1978	28.077	28.084	37.462	37.486

Table A3. (continued)

c)

Year	σ_0 at S_{max}	σ_0 bottom	σ_2 at S_{max}	σ_2 bottom
1982	28.080	28.081	37.466	37.472
1984	28.083	28.0845	37.472	37.485
1988	28.077	28.076	37.460	37.463
1993	28.080	28.079	37.460	37.464
1994	28.080	28.079	37.459	37.463
1995	28.080	28.080	37.457	37.464
1996	28.080	28.080	37.456	37.462
1997	28.078	28.078	37.450	37.460
1998	28.076	28.079	37.448	37.462
1999	28.079	28.080	37.453	37.462
2000	28.079	28.080	37.450	37.461
2001	28.079	28.080	37.449	37.460
2002	28.079	28.081	37.449	37.460
2004	28.081	28.082	37.451	37.459
2005	28.081	28.082	37.452	37.458
2006	28.082	28.083	37.451	37.458
2008	28.083	28.0835	37.452	37.457
2009	28.083	28.084	37.452	37.456
2010	28.083	28.084	37.452	37.456
2013	28.085	28.085	37.453	37.453

[a]Years 1982 and 1993 are from *Meincke et al.* [1997]. (a) Vertical salinity and (b) temperature gradients are computed between the salinity maximum and the deep layer. The vertical diffusion coefficients are from the year above to the year on the row where the value is presented. Densities are presented in (c).

them just enough to fit in most of the waters observed at both sections. Dense waters produced in winter on the Arctic shelves (western Barents Sea and Spitsbergen) due to brine release while the water freezes are present at the FS section during some years (not shown). Those waters have been partly left out since they would not fit into the category of being EBDW or CBDW. A signal of dense water plume in the deep Fram Strait has after the first observations in 1986 [*Quadfasel et al.*, 1988; *Schauer and Fahrbach*, 1999] been observed several times afterwards: e.g., in 1988 and 2002 [*Rudels et al.*, 1999, 2005] and in 2008 [*Jardon et al.*, 2014]. It reached maximal values of salinity (up to 34.945) and was the warmest (θ about -0.67°C) in 2002, while in 2000 and 2008 the water was slightly less saline and colder. The plumes are distinguished from other deep waters as being warmer and more saline, while the density is similar to NDW density thus allowing for the plume waters to mix with the other deep waters present in the Fram Strait.

The northward and southward flows of CBDW estimated are perhaps somewhat larger than expected, and they may be overestimated due to having the other triangle vertices located closer together. The EBDW transports are smaller (Figure 6). At the Fram Strait, the net volume transports of Arctic origin deep waters should be southward, because no other passage exists for waters this deep between the Arctic Ocean and the Nordic Seas. Combining CBDW and EBDW with their small net transports in the Fram Strait, into "Arctic Ocean deep waters" gives an estimate of 0.01 Sv southward and at the GS section 0.02 Sv northward. These numbers are very small and probably an underestimate due to the chosen method. Previous estimates for EBDW transports entering the Greenland Sea gyre by *Meincke et al.* [1997] based on mixing estimates are 0.3 Sv and by *Somavilla et al.* [2013] 0.44 ± 0.09 Sv. In this study, the amount of EBDW range water entering the Greenland Sea gyre is estimated at 0.9 ± 0.6 Sv from mixing estimates. This value is significantly higher than the northward and southward transport estimates for the Arctic Ocean deep waters from geostrophy. However, the water in the EBDW range penetrating from the Greenland slope into the center of the gyre is EBDW that has been strongly diluted by mixing with NDW at the slope between Fram Strait and 75°N [*Rudels et al.*, 2005]. In fact the northward and southward transports of NDW across the 75°N section are estimated from geostrophy as five to ten times larger than the corresponding transports of CBDW and EBDW (Figure 6c). Most of the volume that penetrates into the center of the gyre thus consists of NDW, and if the estimate of 1 Sv is correct, then about 20% of the deep water crossing the 75°N section penetrates into the gyre, while the bulk of the flow takes part in the recirculation in the Greenland Sea and Norwegian Sea gyres. About as much Arctic Ocean deep waters that enter the Greenland Sea gyre from the rim are estimated by Jeansson et al. (personal communication, 2016) to enter the Norwegian Sea. A small fraction of

the deep water will also join the overflow as Norwegian Sea water through the Faroe Bank Channel [*Hansen and Østerhus*, 2000], while the Denmark Strait overflow initially is too light, only allowing the passage of water in the AIW and CBDW density range. The volume transports through the FS and GS sections are thus linked with the processes active in the Greenland Sea gyre.

The local formation of deep water in the Greenland Sea was up to the1980s estimated about 05Sv but has declined to almost zero in the recent decades. Whether an active convection and deep and bottom water formation in the Greenland Sea would intensify the exchanges between the rim and the center, or would the Arctic Ocean deep waters rather bypass the dense central dome in the Greenland Sea as was suggested by Figure 8 in *Rudels* [1995], remains an open question that might perhaps be answered by modelling efforts rather than observations.

Acknowledgments

Thank you to the anonymous reviewer for their helpful comments. This work has received support from the Väisälä Foundation (Marnela), from the EU program NACLIM grant agreement 308299 (Rudels), and from Polish National Science Center, MIXAR grant agreement 2012/05/N/ST10/03643 and Polish-Norwegian Research Program, PAVE grant agreement POL-NOR/202006/10/2013 (Goszczko). Reiner Schlitzer's Ocean Data View (http://odv.awi.de, 2014) was used for studying the Argo data and for the related figures (Figures 2b and 10). The hydrographic data are listed in Table A1a, where WOD data are described and available at http://www.nodc.noaa.gov/OC5/WOD/pr_wod.html, Pangaea data at http://www.pangaea.de/, and for a description and how to access the IPY data see *Stroh et al.* [2015]. Argo data are available and described at http://www.argo.net.

References

Aagaard, K., J. H. Swift, and E. C. Carmack (1985), Thermohaline circulation in the Arctic Mediterranean Seas, *J. Geophys. Res.*, *90*, 4833–4846.

Beszczynska-Möller, A., and S. R. Dye (Eds.) (2013), ICES report on Ocean Climate 2012, *ICES Coop. Res. Rep.*, *321*, 73 pp.

Beszczynska-Möller, A., E. Fahrbach, U. Schauer, and E. Hansen (2012), Variability in Atlantic water temperature and transport at the entrance to the Arctic Ocean, 1997–2010, *ICES J. Mar. Sci.*, *69*, 852–863, doi:10.1093/icesjms/fss056.

Blindheim, J. (1989), Cascading of Barents Sea bottom water into the Norwegian Sea, *Rapp. P.-v. Reun. Cons. Int. Explor. Mer. 188*, 49–58.

Bönisch, G., and P. Schlosser (1995), Deep water formation and exchange rates in the Greenland/Norwegian Seas and the Eurasian Basin of the Arctic Ocean derived from tracer balances, *Prog. Oceanogr.*, *35*, 29–52.

Bönisch, G., J. Blindheim, J. L. Bullister, P. Schlosser, and D. W. R. Wallace (1997). Long-term trends of temperature, salinity, density, and transient tracers in the central Greenland Sea, *J. Geophys. Res.*, *102*, 18,553–18,571.

Borenäs, K. M., and P. A. Lundberg (1988), On the deep-water flow through the Faroe Bank Channel, *J. Geophys. Res.*, *93*, 1281–1292.

Bourke, R. H., A. M. Weigel, and R. G. Paquette (1988), The westward turning branch of the West Spitsbergen Current, *J. Geophys. Res.*, *93*, 14,065–14,077.

Buch, E., S.-A. Malmberg, and S.S. Kristmansson (1996), Arctic Ocean deep water masses in the western Iceland Sea, *J. Geophys. Res.*, *101*, 11,965–11,973.

Budéus, G., and S. Ronski (2009), An integral view of the hydrographic development in the Greenland Sea over a decade. *Open Oceanogr. J.*, *3*, 8–39.

Budéus, G., W. Schneider, and G. Krause (1998), Winter convective events and bottom water warming in the Greenland Sea, *J. Geophys. Res.*, *103*, 18,513–18,527.

Cisewski, B., G. Budéus, and G. Krause (2003), Absolute transport estimates of total and individual water masses in the northern Greenland Sea derived from hydrographic and acoustic Doppler current profiler measurements, *J. Geophys. Res.*, *108*(C9), 3298, doi:10.1029/2002JC001530.

de Steur, L., E. Hansen, R. Gerdes, M. Karcher, E. Fahrbach, and J. Holfort (2009), Freshwater fluxes in the East Greenland Current: A decade of observations. *Geophys. Res. Lett.*, *36*, L23611, doi:10.1029/2009GL041278.

de Steur, L., E. Hansen, C. Mauritzen, A. Beszczynska-Möller, and E. Fahrbach (2014), Impact of Recirculation on the East Greenland Current: Results from moored current meter measurements between 1997 and 2009, *Deep Sea Res., Part I*, *92*, 26–40, doi:10.1016/j.dsr.2014.05.018.

Dooley, H. D., and J. Meincke (1981), Circulation and water masses in the Faroese Channels during overflow '73. *Dtsch. Hydrogr. Z.*, *34*, 4–54.

Fahrbach, E., J. Meincke, S. Østerhus, G. Rohardt, U. Schauer, V. Tverberg, and J. Verduin (2001), Direct measurements of volume transports through Fram Strait, *Polar Res.*, *20*, 217–224.

Fieg, K., R. Gerdes, E. Fahrbach, A. Beszczynska-Möller, and U. Schauer (2010), Simulation of oceanic volume transports through Fram Strait 1995–2005, *Ocean Dyn.*, *60*, 491–502, doi:10.1007/s10236-010-0263-9.

Gascard, J.-C., A. J. Watson, M.-J. Messias, K. A. Olsson, T. Johannessen, and K. Simonsen (2002), Long-lived vortices as a mode of deep ventilation in the Greenland Sea, *Nature*, *416*, 525–527.

Hansen, B., and S. Østerhus (2000), North Atlantic: Nordic seas exchanges, *Prog. Oceanogr.*, *45*, 109–208.

Hansen, B., K. M. H. Larsen, H. Hátún, R. Kristiansen, E. Mortensen, and S. Østerhus (2015), Increasing transports of volume, heat, and salt towards the Arctic in the Faroe Current 1993–2013, *Ocean Sci. Discuss.*, *12*, 1013–1050. doi:10.5194/osd-12-1013-2015.

Houssais, M.-N., B. Rudels, H. Friedrich, and D. Quadfasel (1995), Exchanges through Fram Strait, in *Nordic Seas Symposium on the Results of the Greenland Sea Project (GSP) 1987–1993, Extended Abstracts*, edited by J. Meincke, pp. 87–91, Hamburg.

Ingvaldsen, R. B., L. Asplin, H. Loeng, (2004), The seasonal cycle in the Atlantic transport to the Barents Sea during 1997–2001, *Cont. Shelf Res.*, *24*, 1015–1032. doi:10.1016/j.csr.2004.02.01.

Jacobsen, J. P., and A. J. C. Jensen (1926), Examination of hydrographical measurements from the research vessels Explorer and Dana during the summer of 1924, *Rapp. P. V. Cons. Perm. Int. Explor. Mer.*, *39*, 31–84.

Jardon, F. P., F. Vivier, P. Bouruet-Aubertot, A. Lourenço, Y. Cuypers, and S. Willmes (2014), Ice production in Storfjorden (Svalbard) estimated from a model based on AMSR-E observations: Impact on water mass properties, *J. Geophys. Res. Oceans*, *119*, 377–393, doi:10.1002/2013JC009322.

Jonsson, S., and H. Valdimarsson (2004), A new path for the Denmark Strait overflow water from the Iceland Sea to Denmark Strait, *Geophys. Res. Lett.*, *31*, L03305, doi:10.1029/2003GLO19214.

Karstensen, J., P. Schlosser, D. W. R. Wallace, J. L. Bullister, and J. Blindheim (2005), Water mass transformation in the Greenland Sea during the 1990s, *J. Geophys. Res.*, *110*, C07022, doi:10.1029/2004JC002510.

Klenke, M., and Schenke (2002), A new bathymetric model for the central Fram Strait, *Mar. Geophys. Res.*, *23*, 367–378.

Lanczos, C. (1970), *The Variational Principles of Mechanics*, 4th ed., 418 pp., Univ. of Toronto Press, Toronto.

Langehaug, H. R., and E. Falck (2012), Changes in the properties and distribution of the intermediate and deep waters in the Fram Strait, *Prog. Oceanogr.*, *96*, 57–76, doi:10.1016/j.pocean.2011.10.002.

Latarius, K. (2013), Über die Wassermassentransformation im Europäischen Nordmeer: Prozess-Studien und Budgets, PhD dissertation, 170 pp., Univ. of Hamburg, Hamburg, Germany.
Latarius, K., and D. Quadfasel (2010), Seasonal to inter-annual variability of temperature and salinity in the Greenland Sea Gyre: Heat and freshwater budgets, *Tellus Ser. A*, *62*, 497–515, doi:10.1111/j.1600-0870.2010.00453.x.
Mamayev, O. I. (1975), *Temperature-Salinity Analysis of World Ocean Waters*, 374 p., Elsevier Sci., Amsterdam, Oxford.
Manley, T. O. (1995), Branching of Atlantic water within the Greenland-Spitsbergen Passage: An estimate of recirculation, *J. Geophys. Res.*, *100*, 20,627–20,634.
Marnela, M., B. Rudels, M.-N. Houssais, A. Beszczynska-Möller, and P.B. Eriksson (2013), Recirculation in the Fram Strait and transports of water in and north of the Fram Strait derived from CTD data. *Ocean Sci.*, *9*, 499–519. doi:10.5194/os-9-499-2013.
Mauritzen, C. (1996a), Production of dense overflow waters feeding the North Atlantic across the Greenland–Scotland Ridge. Part 1: Evidence for a revised circulation scheme, *Deep Sea Res., Part I*, *43*, 769–806.
Mauritzen, C. (1996b), Production of dense overflow waters feeding the North Atlantic across the Greenland–Scotland Ridge. Part 2: An inverse model, *Deep Sea Res., Part I*, *43*, 807–835.
Meincke, J., B. Rudels, and H. J. Friedrich (1997), The Arctic Ocean: Nordic Seas thermohaline system, *ICES J. Mar. Sci.*, *54*, 283–299, doi: 10.1006/jmsc.1997.0229.
Moore, G. W. K., K. Våge, R. S. Pickart, and I. A. Renfrew (2015). Decreasing intensity of open-ocean convection in the Greenland and Iceland seas, *Nat. Clim. Change, in press.*
Nansen, F. (1902), *Oceanography of the North Polar Basin, The Norwegian North Polar Expedition 1893-1896, Sci. Results 9*, 427 pp.
Oliver, K. I. C., T. Eldevik, D. P. Stevems, and A. J. Watson (2008), A Greenland Sea perspective on the dynamics of postconvective eddies, *J. Phys. Oceanogr.*, *38*, 2755–2771, doi:10.1175/2008JPO3844.1.
Quadfasel, D., and J. Meincke (1987), Note on the thermal structure of the Greenland Sea gyres, *Deep Sea Res., Part A*, *34*, 1883–1888.
Quadfasel, D., B. Rudels, and K. Kurz (1988), Outflow of dense water from a Svalbard fjord into the Fram Strait, *Deep Sea Res., Part A*, *35*, 1143–1150.
Rahmstorf, S. (1995), Bifurcation of the Atlantic thermohaline circulation in response to changes in the hydrological cycle, *Nature*, *378*, 145–149.
Ronski, S., and G. Budéus (2005), Time series of winter convection in the Greenland Sea, *J. Geophys. Res. Oceans*, *110*, C04015, doi:10.1029/2004JC002318.
Rudels, B. (1986), The θ-S relations in the northern seas: Implications for the deep circulation, *Polar Res.*, *4*, 133–159.
Rudels, B. (1987), *On the Mass Balance of the Polar Ocean, with Special Emphasis on the Fram Strait*, 188 p., Norsk Polarinstitutt Skr., Oslo.
Rudels, B. (1995), The thermohaline circulation of the Arctic Ocean and the Greenland Sea, *Philos. Trans. R. Soc. London A*, *352*, 287–299.
Rudels, B. (2010), Constraints on exchanges in the Arctic Mediterranean: Do they exist and can they be of use?, *Tellus Ser. A*, *62*, 109–122, doi:10.1111/j.1600-0870.2009.00425.x.
Rudels, B., P. Eriksson, H. Grönvall, R. Hietala, and J. Launiainen (1999), Hydrographic observations in Denmark Strait in fall 1997, and their implications for the entrainment into the overflow plume, *Geophys. Res. Lett.*, *26*, 1325–1328.
Rudels, B., G. Björk, J. Nilsson, P. Winsor, I. Lake, and C. Nohr (2005), The interaction between waters from the Arctic Ocean and the Nordic Seas north of Fram Strait and along the East Greenland Current: Results from the Arctic Ocean-02 Oden expedition, *J. Mar. Syst.*, *55*, 1–30.
Rudels, B., M. Marnela, and P. Eriksson (2008), Constraints on Estimating mass, heat and freshwater transports in the Arctic Ocean: An exercise, in *Arctic-Subarctic Ocean Fluxes*, edited by R. R Dickson, J. Meincke, and P. Rhines, pp. 315–341, Springer, Dordrecht, Netherlands.
Rudels, B., M. Korhonen, G. Budéus, A. Beszczynska-Möller, U. Schauer, A. Nummelin, D. Quadfasel, and H. Valdimarsson (2012), The East Greenland Current and its impacts on the Nordic Seas: Observed trends in the past decade, *ICES J. Mar. Sci.*, *69(5)*, 84-–851, doi:10.1093/icesjms/fss079.
Rudels, B., U. Schauer, G. Björk, M. Korhonen, S. Pisarev, B. Rabe, and A. Wisotzki (2013), Observations of water masses and circulation with focus on the Eurasian Basin of the Arctic Ocean from the 1990s to the late 2000s, *Ocean Sci.*, *9*(1), 147–169.
Ryder, C. (1891−1892), Tidligere Ekspeditioner til Grønlands Østkyst nordfor 66° Nr. Br, *Geogr. Tids. Bd.*, *11*, pp. 62–107, København.
Schauer, U., and A. Beszczynska-Möller (2009), Problems with estimation and interpretation of oceanic heat transport: Conceptual remarks for the case of Fram Strait in the Arctic Ocean, *Ocean Sci.*, *5*, 487–494, doi:10.5194/os-5-487-2009.
Schauer, U., and E. Fahrbach (1999), A dense bottom water plume in the western Barents Sea: Downstream modification and interannual variability, *Deep Sea Res., Part I*, *46*, 2095–2108.
Smethie, W. M., Jr., and J. H. Swift (1989), The tritium-krypton-85 age of Denmark Strait overflow water and Gibbs Fracture Zone water just south of Denmark Strait, *J. Geophys. Res.*, *94*, 8265–8275.
Somavilla, R., U. Schauer, and G. Budéus (2013), Increasing amount of Arctic Ocean deep waters in the Greenland Sea, *Geophys. Res. Lett.*, *40*, 4361–4366, doi:10.1002/grl.50775.
Stommel, H. (1961), Thermohaline convection with two stable regimes of flow, *Tellus*, *13*, 224–230.
Stommel, H. and G. Veronis (1981), Variational inverse method for study of ocean circulation, *Deep Sea Res., Part A*, *28*, 1147–1160.
Stroh, J. N., G. Panteleev, S. Kirillov, M. Makhotin, and N. Shakhova (2015), Sea-surface temperature and salinity product comparison against external in situ data in the Arctic Ocean, *J. Geophys. Res. Oceans*, *120*, 7223–7236, doi:10.1002/2015JC011005.
Swift, J. H., and K. Aagaard (1981), Seasonal transitions and water mass formation in the Icelandic and Greenland Seas, *Deep Sea Res., Part A*, *28*, 1107–1129.
Swift, J. H., and K. P. Koltermann (1988), The origin of Norwegian Sea deep water. *J. Geophys. Res.*, *93*, 3563–3569.
Swift, J. H., K. Aagaard, and S.-A. Malmberg, (1980), The contribution of the Denmark Strait overflow to the deep North Atlantic, *Deep Sea Res., Part A*, *27*, 29–42.
Tsubouchi, T., S. Bacon, A. C. Naveira Garabato, Y. Aksenov, S. W. Laxon, E. Fahrbach, A. Beszczynska-Möller, E. Hansen, C. M. Lee, and R. B. Ingvaldsen (2012), The Arctic Ocean in summer: A quasi-synoptic inverse estimate of boundary fluxes and water mass transformation, *J. Geophys. Res.*, *117*, C01024, doi:10.1029/2011JC007174.
Visbeck, M., J. Fischer, and F. Schott (1995), Preconditioning the Greenland Sea for deep convection: Ice formation and ice drift, *J. Geophys. Res.*, *100*, 18,489–18,502.
Voet, G., D. Quadfasel, K. A. Mork, and H. Søiland (2010), The mid-depth circulation of the Nordic Seas derived from profiling float observations, *Tellus Ser. A*, *62*, 516–529, doi:10.1111/j.1600-0870.2010.00444.x.
von Appen, W.-J., U. Schauer, R. Somavilla, E. Bauerfeind, and A. Beszczynska-Möller (2015), Exchange of warming deep waters across Fram Strait, *Deep Sea Res., Part I*, *103*, 86–100, doi:10.1016/j.dsr.2015.06.003.

Walczowski, W., J. Piechura, I. Goszczko, and P. Wieczorek (2012), Changes in Atlantic water properties: An important factor in the European Arctic marine climate, *ICES J. Mar. Sci.*, *69(5)*, 864–869, doi:10.1093/icesjms/fss068.

Wang, X., J. Zhao, T. Li, W. Zhong, and Y. Jiao (2015), Deep waters warming in the Nordic seas from 1972 to 2013, *Acta Oceanol. Sin.*, *34*(3), 18–24, doi:10.1007/s13131-015-0613-z.

Wessel, P., and Smith, W. H. F. (1998), New, improved version of Generic Mapping Tools released, *EOS Trans. AGU.*, *79*, p. 579, doi:10.1029/98EO00426.

Wunsch, C. (1978), The North Atlantic general circulation west of 50_W determined by inverse methods, *Revs. Geophys. Space Phys.*, *16*, 583–620.